Numerical models for earthquake ground motion

Alfio Quarteroni
MOX, Politecnico di Milano
and EPFL, Lausanne (professor emeritus)

SIAM Conference on
Mathematical & Computational Issues in the Geosciences (GS19)
March 11 - 14, 2019
Houston, Texas, USA

POLITECNICO MILANO 1863

MODELLISTICA E CALCOLO SCIENTIFICO
MOX
MODELING AND SCIENTIFIC COMPUTING

ÉCOLE POLYTECHNIQUE FÉDÉRALE DE LAUSANNE

CMCS

Acknowledgements: the SPEED group

R. Paolucci
DICA, PoliMI

P. Antonietti
MOX, PoliMI

M. Stupazzini
Munich RE

I. Mazzieri
MOX, PoliMI

C. Smerzini
DICA, PoliMI

F. Bonaldi
MOX, PoliMI

Ali Ozcebe
DICA, PoliMI

L. Melas
MOX, PoliMI

F. Migliorini
MOX, PoliMI

M. Infantino
DICA, PoliMI

F. Gatti
Paris Supélec

POLITECNICO
MILANO 1863

SPEED

http://speed.mox.polimi.it

Munich RE

Percentage distribution for relevant natural loss events worldwide 1980 – 2017

NatCatSERVICE

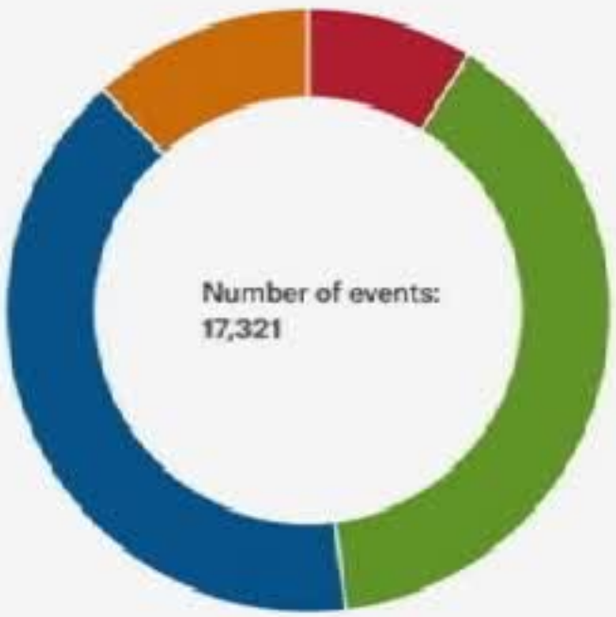

- 8.9 %
- 39.1 %
- 40.1 %
- 11.9 %

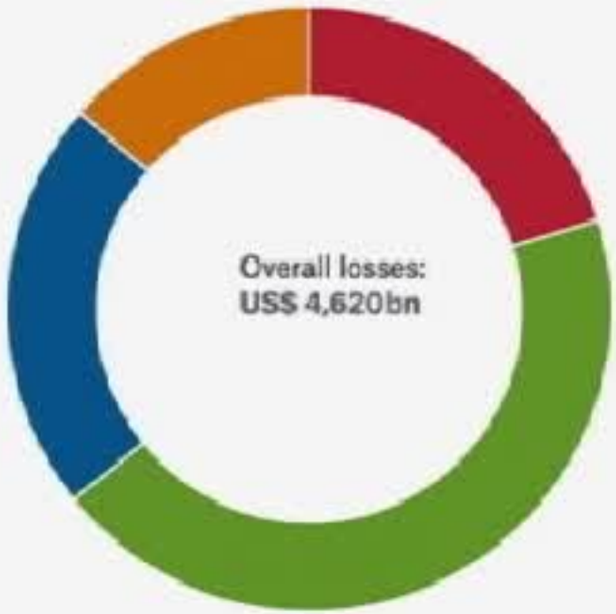

- 20.2 %
- 44 %
- 22.1 %
- 13.7 %

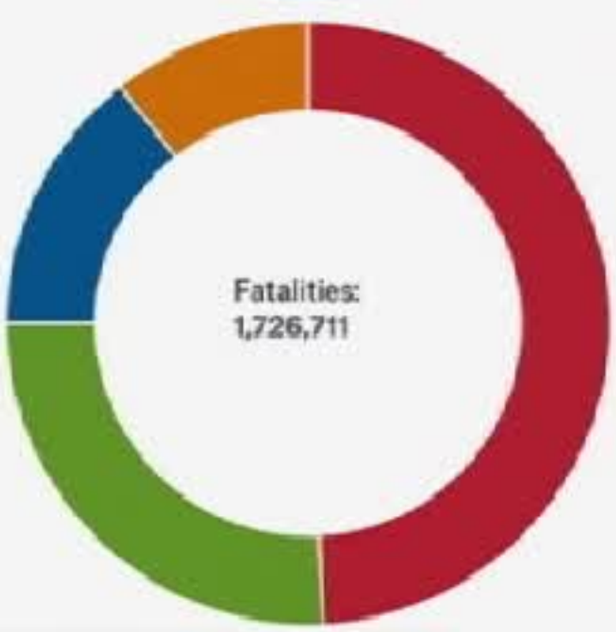

- 49.2 %
- 25.8 %
- 14.3 %
- 10.7 %

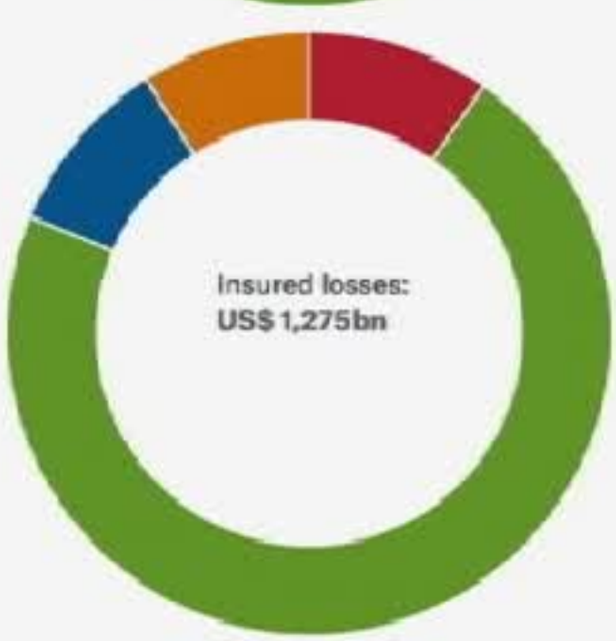

- 9.8 %
- 71.5 %
- 9.6 %
- 9.1 %

Munich RE

- **Geophysical events** (Earthquake, tsunami, volcanic activity)
- **Meteorological events** (Tropical storm, extratropical storm, convective storm, local storm)
- **Hydrological events** (Flood, mass movement)
- **Climatological events** (Extreme temperature, drought, forest fire)

● Geophysical events ● Meteorological events ● Hydrological events ● Climatological events

Major events and losses in 2016

NatCatSERVICE

Loss events worldwide 2016

Geographical overview

Munich RE

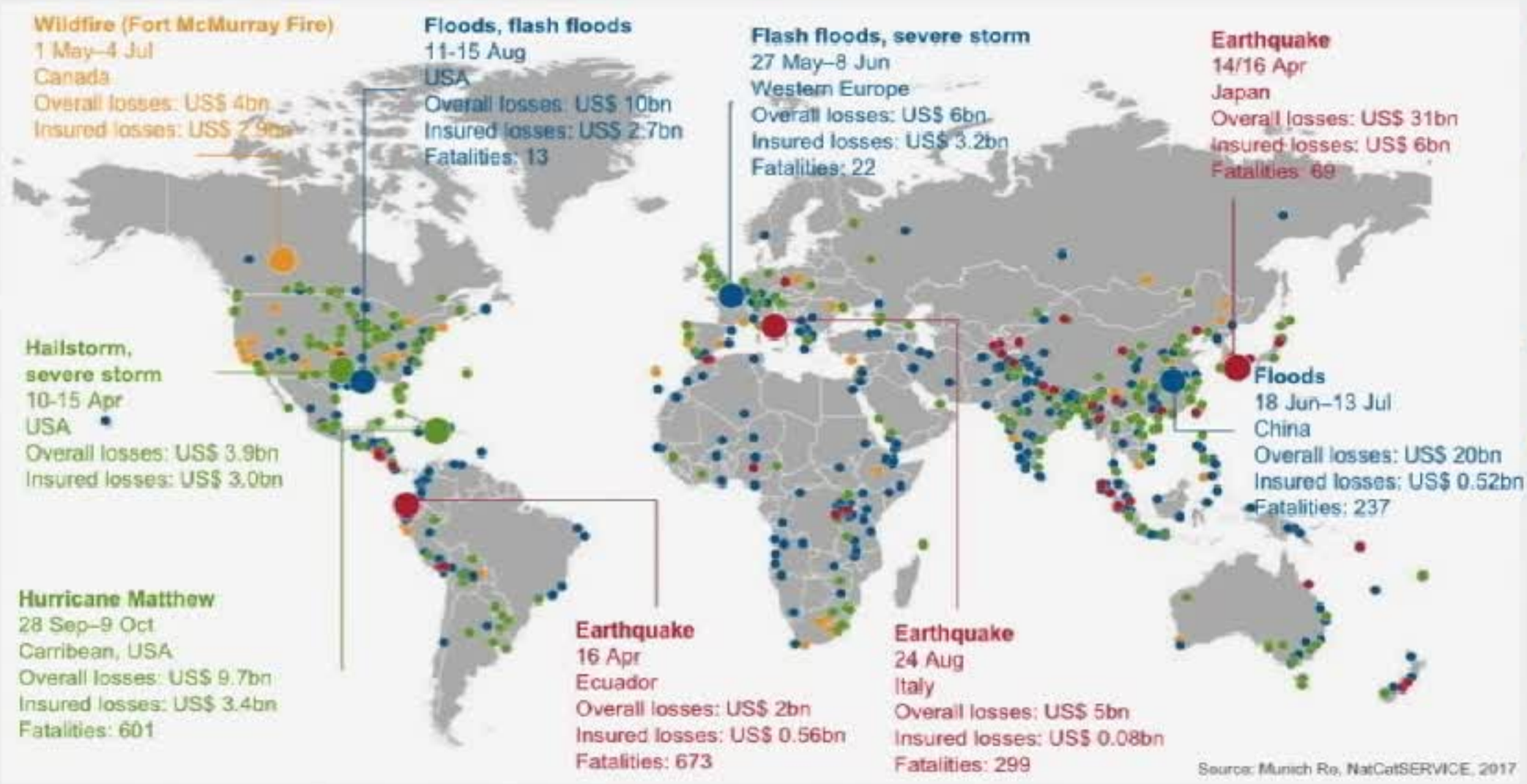

- **Geophysical events** (Earthquake, tsunami, volcanic activity)
- **Meteorological events** (Tropical storm, extratropical storm, convective storm, local storm)
- **Hydrological events** (Flood, mass movement)
- **Climatological events** (Extreme temperature, drought, wildfire)

10 Deadliest Events - Past 35 Years

NatCatSERVICE

Significant loss events worldwide 1980 – 2016

10 deadliest events

Date	Event	Affected area	Overall losses in US$ m original values	Insured losses in US$ m original values	Fatalities
26.12.2004	Earthquake, tsunami	Sri Lanka, Indonesia, Thailand, India, Bangladesh, Myanmar, Maldives, Malaysia	10,000	1,000	**220,000**
12.1.2010	Earthquake	Haiti	8,000	200	**159,000**
2-5.5.2008	Cyclone Nargis	Myanmar	4,000		**140,000**
29-30.4.1991	Tropical cyclone	Bangladesh	3,000	100	**139,000**
8.10.2005	Earthquake	Pakistan, India, Afghanistan	5,200	5	**88,000**
12.5.2008	Earthquake	China	85,000	300	**84,000**
July - Aug 2003	Heat wave	Europe	14,000	1,100	**70,000**
July - Sep 2010	Heat wave	Russian Federation			**56,000**
20.6.1990	Earthquake	Iran	7,100	100	**40,000**
26.12.2003	Earthquake	Iran	500	20	**26,200**

Source: Munich Re, NatCatSERVICE, 2017

Earthquakes in a nutshell

An earthquake is the shaking of the surface of the Earth, resulting from the sudden release of energy in the Earth's lithosphere.

This energy has built up over long periods of time as a result of tectonic forces within the earth.

Sudden release of energy causes seismic waves to radiate from their point of origin through the earth. Seismic waves produce ground motion.

The seismicity of an area is expressed by the frequency, type and size of earthquakes experienced over a period of time.

Hypocenter (focus): earthquake's point of initial rupture.

Epicenter: the point at ground level directly above the hypocenter.

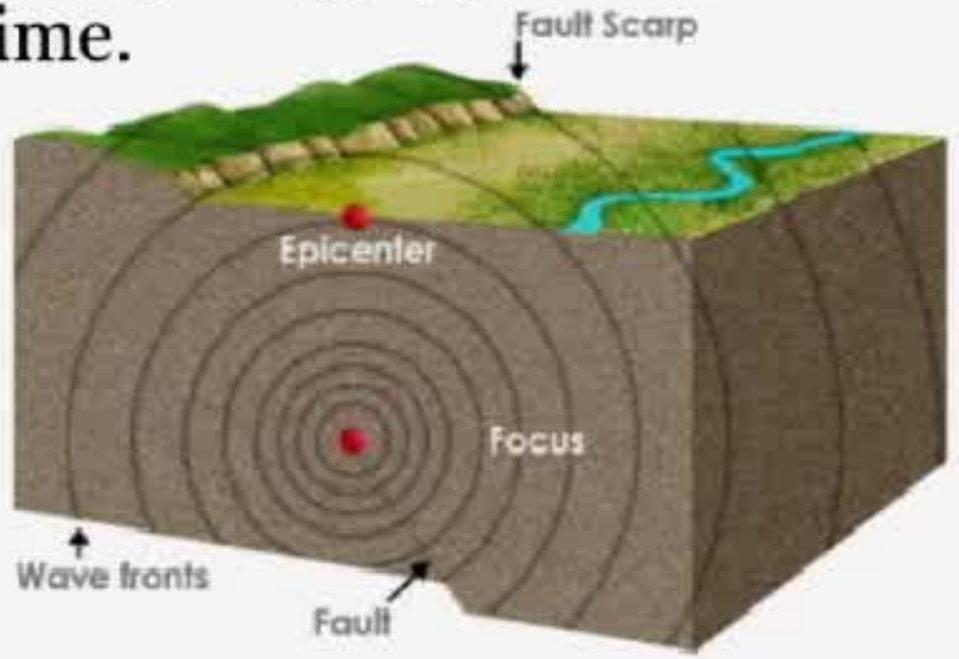

Geodynamics: P and S waves

P waves (compressional/primary waves)

The particles in the solid vibrate along the axis of propagation (the direction of motion) of the wave.

These waves can travel through any type of material, including fluids

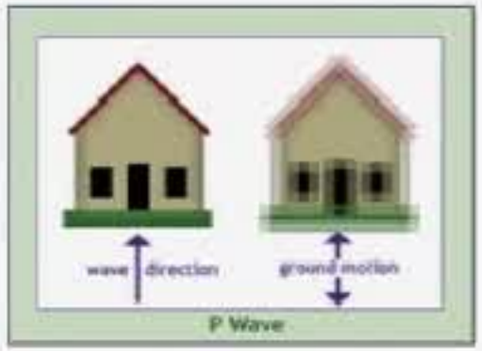

S waves (shear/transverse waves)

The motion is perpendicular to the direction of wave propagation.

These waves can travel through solid media

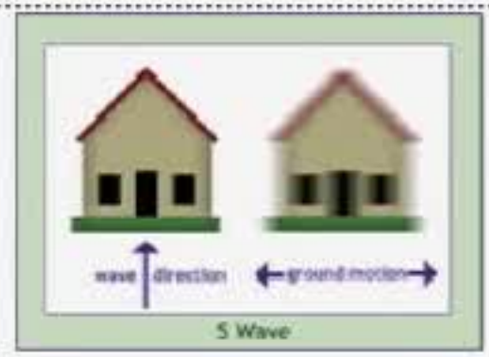

Love waves

The particle motion forms a horizontal line perpendicular to the direction of propagation.

Travel with a lower velocity than P- or S- waves, but faster than Rayleigh waves

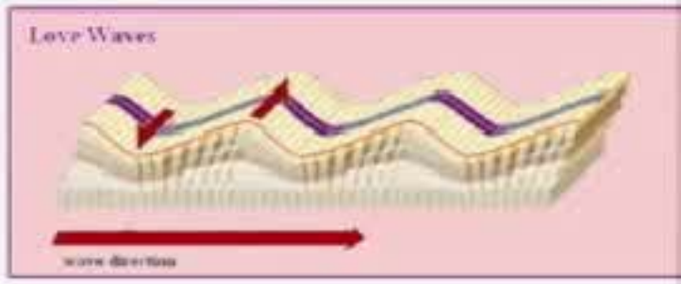

Rayleigh waves

In isotropic solids Rayleigh waves cause the surface particles to move in ellipses in planes normal to the surface and parallel to the direction of propagation

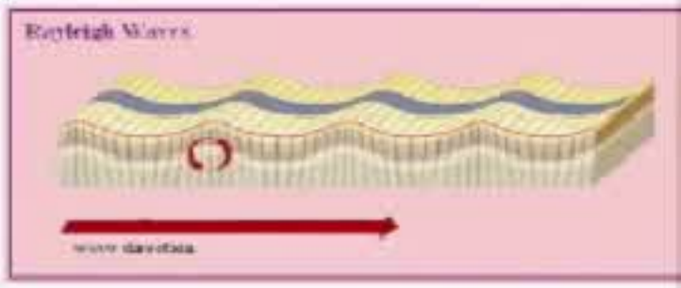

Speed of p and s waves

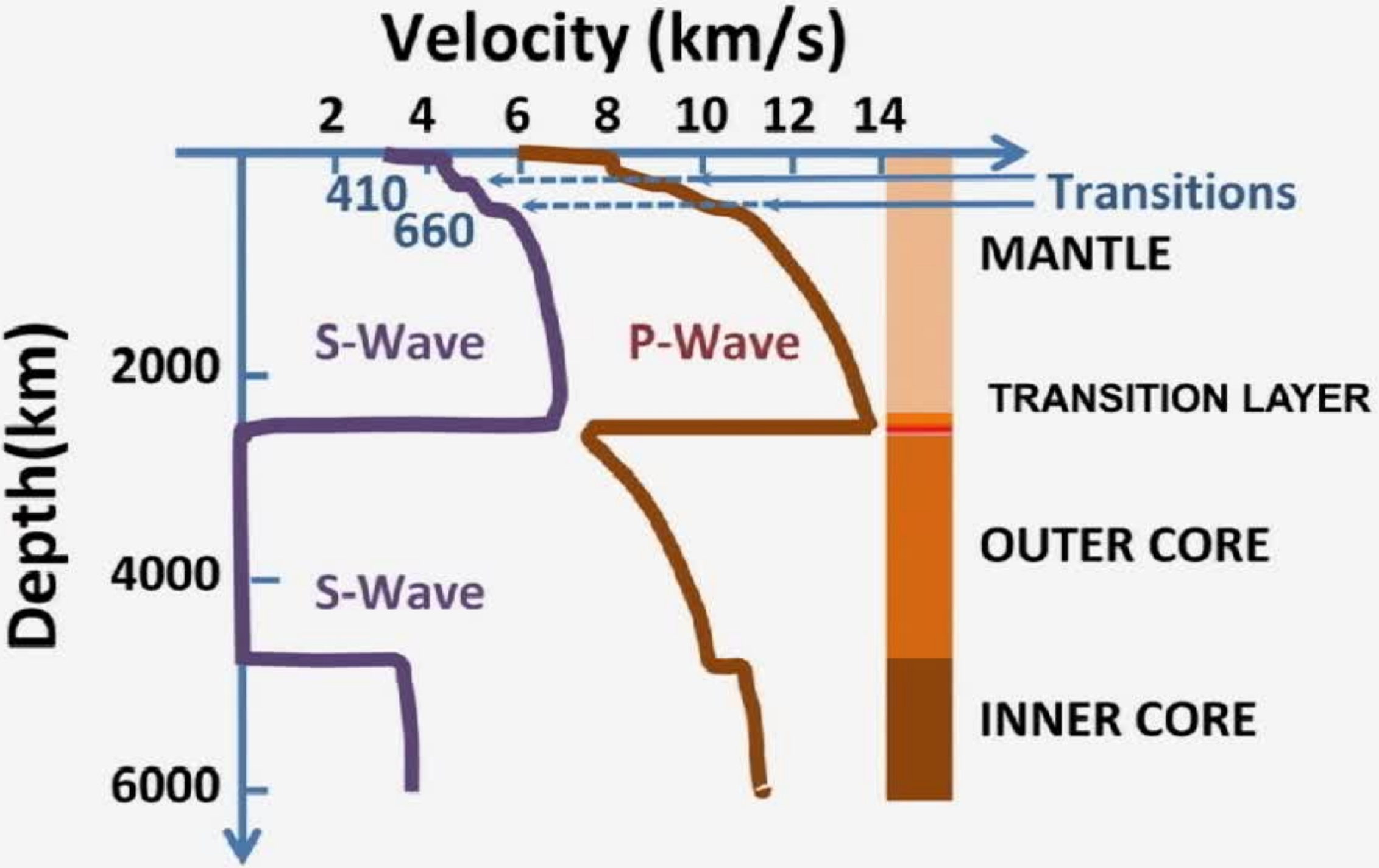

[Helffrich ,Wood, "The Earth's Mantle", Nature, 2002]

Measuring the size of an earthquake

The magnitude is a number that characterises the relative size of an earthquake. It is based on measurement of the maximum motion recorded by a seismograph.

Different scales to measure earthquake magnitude:

the moment magnitude (Mw) scale is based on the concept of seismic moment. It is uniformly applicable to all sizes of earthquakes.

$$M_w = \frac{2}{3} log_{10} M_0 - 10.7$$

M_0: Seismic moment at the epicenter [N · m].
(~area of the rupture along the geologic fault where the earthquake occurred × average displacement)

An increase of one step on the logarithmic scale corresponds to a $10^{1.5} \approx 32$ times increase in the amount of energy released

The moment magnitude scale was introduced to address some shortcomings of the Richter scale while maintaining consistency for medium-sized earthquakes

Hazard, vulnerability, and exposure

Seismic hazard: probability that an earthquake will occur in a given geographic area, within a given window of time, and with ground motion intensity exceeding a given threshold.

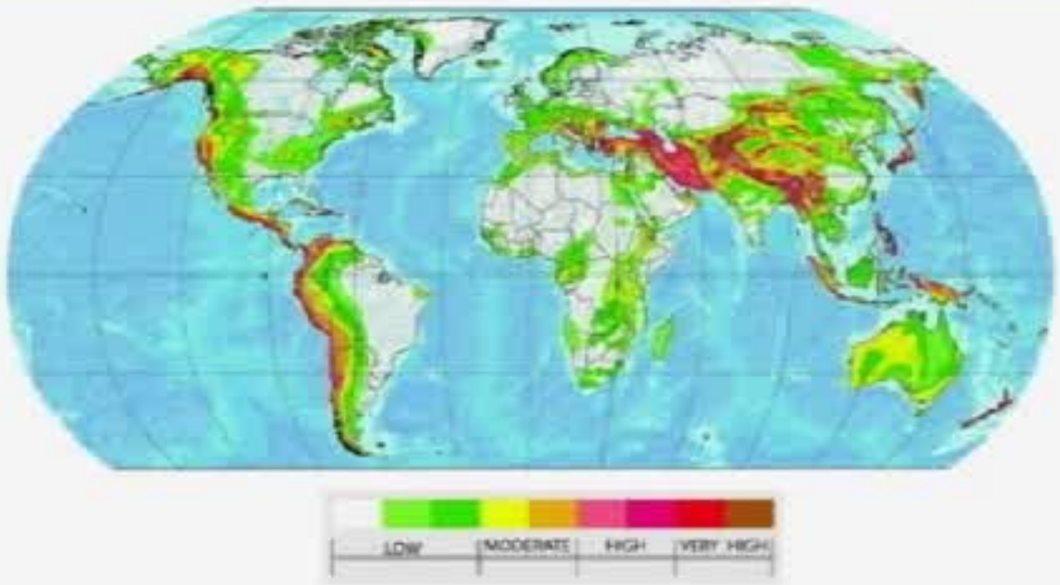

Vulnerability

Seismic vulnerability: resistance of buildings to the effects of a seismic tremor (due to type, design, poor quality materials and construction methods, lack of maintenance).

Exposure

Seismic exposure: possibility of damage, in economic terms, to cultural heritage or the loss of human lives

Seismic risk

(See Parthenon's seismic risk analysis later

Seismic risk: measurement of the damage expected in a given interval of time, determined by the combination of hazard, vulnerability and exposure

Overview of methods for Ground Motion Prediction - GMP

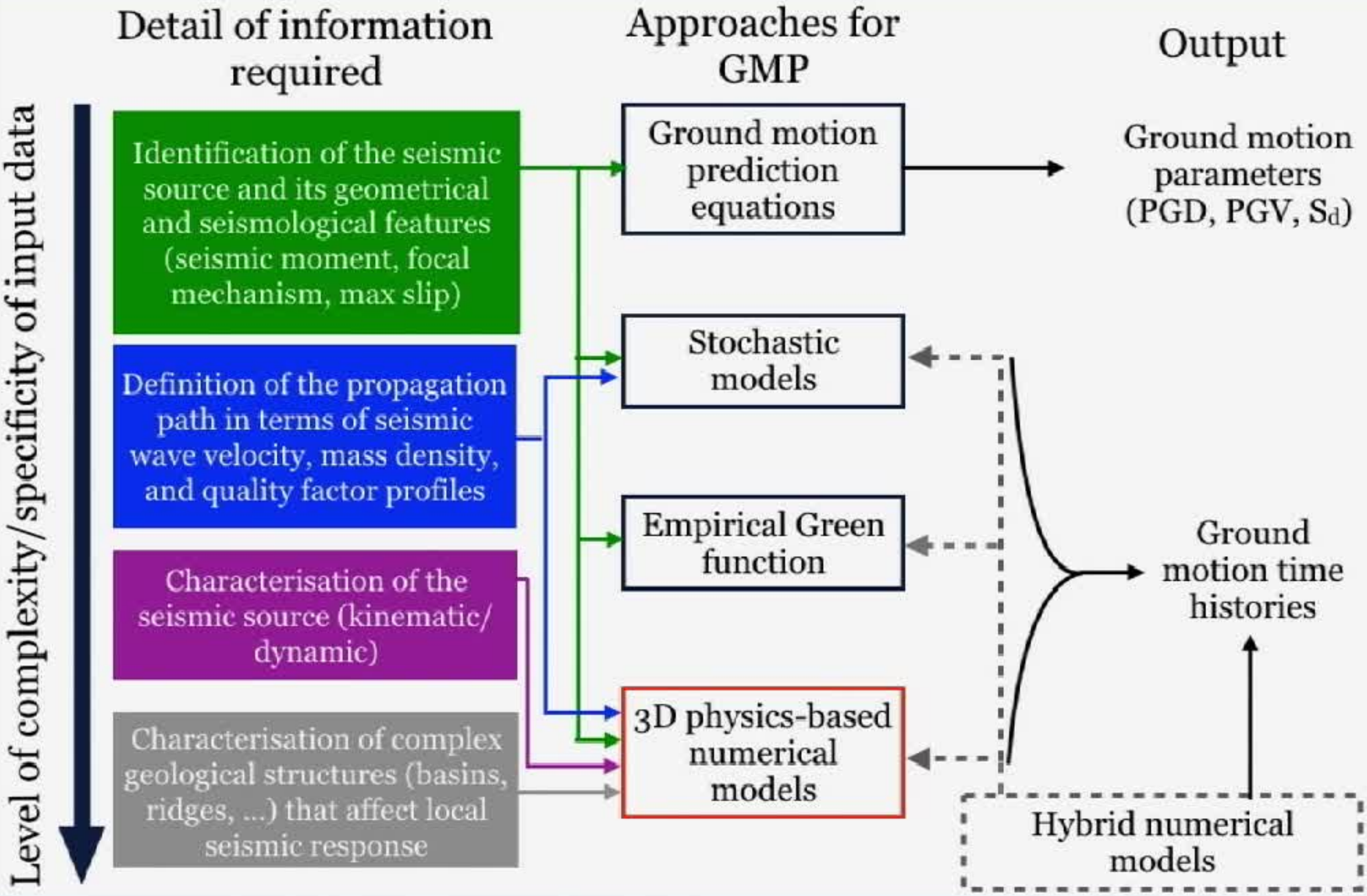

One limitation of GMPEs

Recorded near-fault ground motions as a function of the site distance from epicentre (x-axis) and the magnitude (y-axis)

Physics-based simulations to improve GMPE calibration

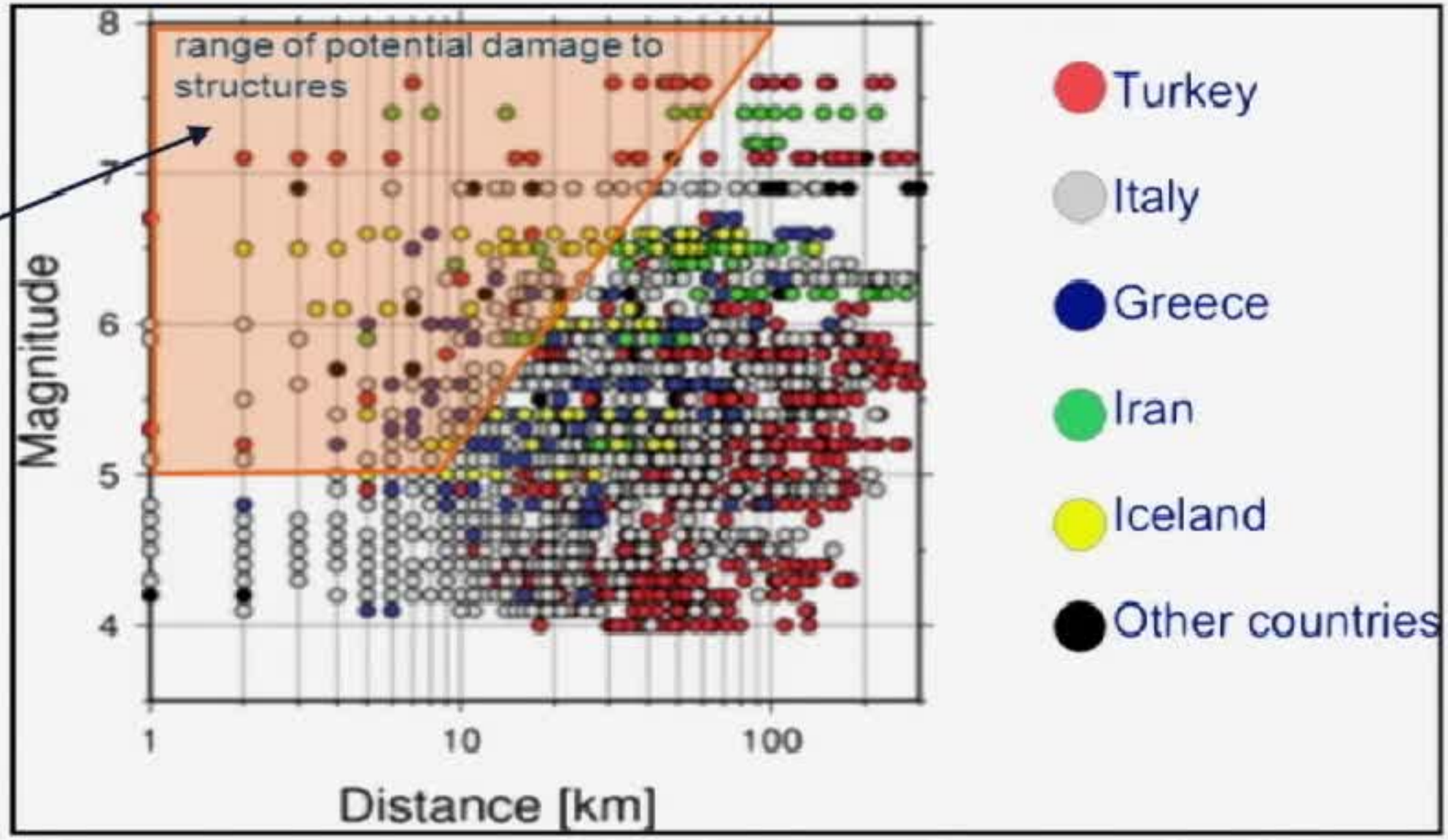

Magnitude and distance range covered by the ground motion database for calibration of pan-European ground motion prediction equations.

Main limitations of GMPEs: poor calibration in the near-source region

Workflow overview of seismic risk analysis

Earthquake input data (magnitude, fault dynamics, topography, soil type, …)

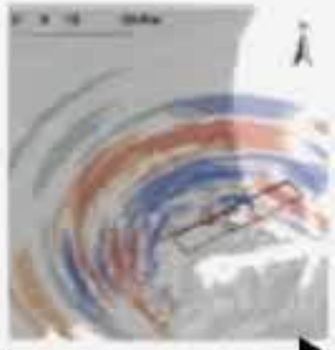

Peak ground velocity, spectral displacement, …

Investigation of the risk of the damage from an earthquake to a builiding

3D physics-based scenarios

+

Ground motion parameters

+

Fragility curves

=

Seismic risk analysis

Displacement field: solution of elastodynamics equations with SPEED

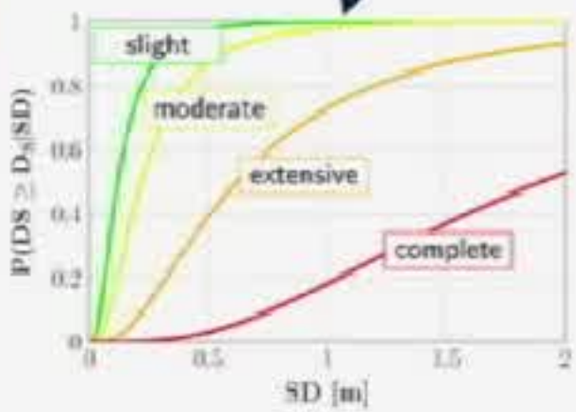

Probability of reaching a damage state for a given seismic response parameter

The mathematical model
and
its numerical approximation

The mathematical model

Governing equations for the displacement $\mathbf{u}(\mathbf{x}, t)$ of a dynamically disturbed elastic medium:

Law of momentum conservation

$$\rho\ddot{\mathbf{u}} - \nabla \cdot \underline{\sigma}(\mathbf{u}) + G(\mathbf{u}) = \mathbf{f} \quad \text{in } \Omega \times (0, T]$$

where

- $\mathbf{u}$ is the displacement field
- ρ is the medium density

$$G(\mathbf{u}) = \begin{cases} \mathbf{0} & \text{fully elastic} \\ 2\rho\zeta\dot{\mathbf{u}} + \rho\zeta^2\mathbf{u} & \text{viscoelastic} \end{cases}$$

$\zeta \geq 0$ is a damping factor ($\sim 0.01 s^{-1}$)

Constitutive laws

– Hookes' law

$$\underline{\sigma}(\mathbf{u},t) = \underline{\underline{\mathbb{D}}}\,\underline{\varepsilon}(\mathbf{u}) \equiv \lambda \mathrm{tr}(\underline{\varepsilon}(\mathbf{u}))\underline{\underline{I}} + 2\mu\underline{\varepsilon}(\mathbf{u},t)$$

$\lambda = \lambda(\mathbf{x})$ and $\mu = \mu(\mathbf{x})$ are the first and second Lame' elastic coefficients

– Non-linear elastic

$$\underline{\sigma}(\mathbf{u},t) = \underline{\underline{\mathbb{D}}}(\lambda,\mu)\underline{\varepsilon}(\mathbf{u}) \longrightarrow \quad \lambda = \lambda(\mathbf{x}) \quad \mu = \mu(\mathbf{x},t,\underline{\varepsilon}(\mathbf{u}))$$

– Viscoelastic

$$\underline{\sigma}(\mathbf{u},t) = \underline{\underline{\mathbb{D}}}(\mathbf{x},0)\underline{\varepsilon}(\mathbf{u},t) - \int_0^t \frac{\partial \underline{\underline{\mathbb{D}}}}{\partial s}(\mathbf{x},t-s)\underline{\varepsilon}(\mathbf{u},s)\mathrm{d}s$$

Computational domain and boundary conditions

$$\begin{cases} \nabla \cdot \underline{\sigma}(\mathbf{u})\mathbf{n} = \mathbf{t} & \text{on } \Gamma_N \times (0,T] \\ \text{Non reflecting BCs} & \text{on } \Gamma_{NR} \times (0,T] \end{cases}$$

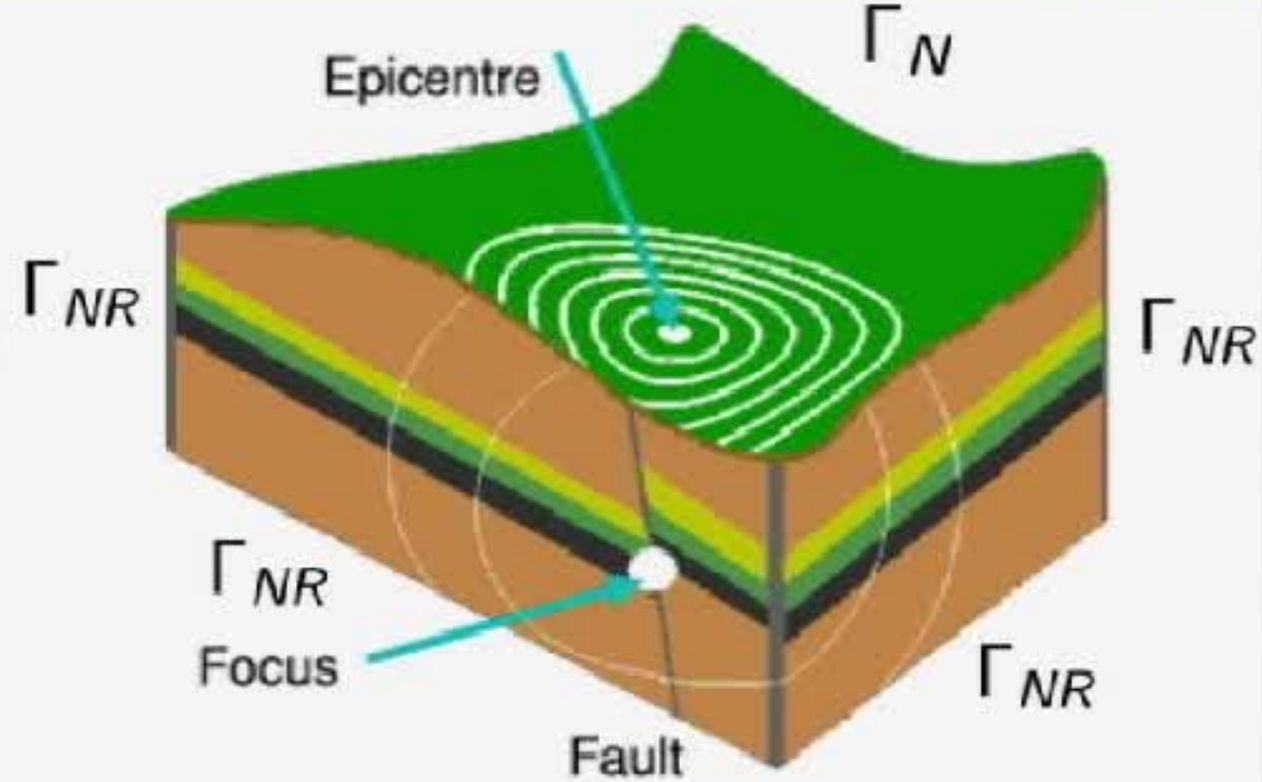

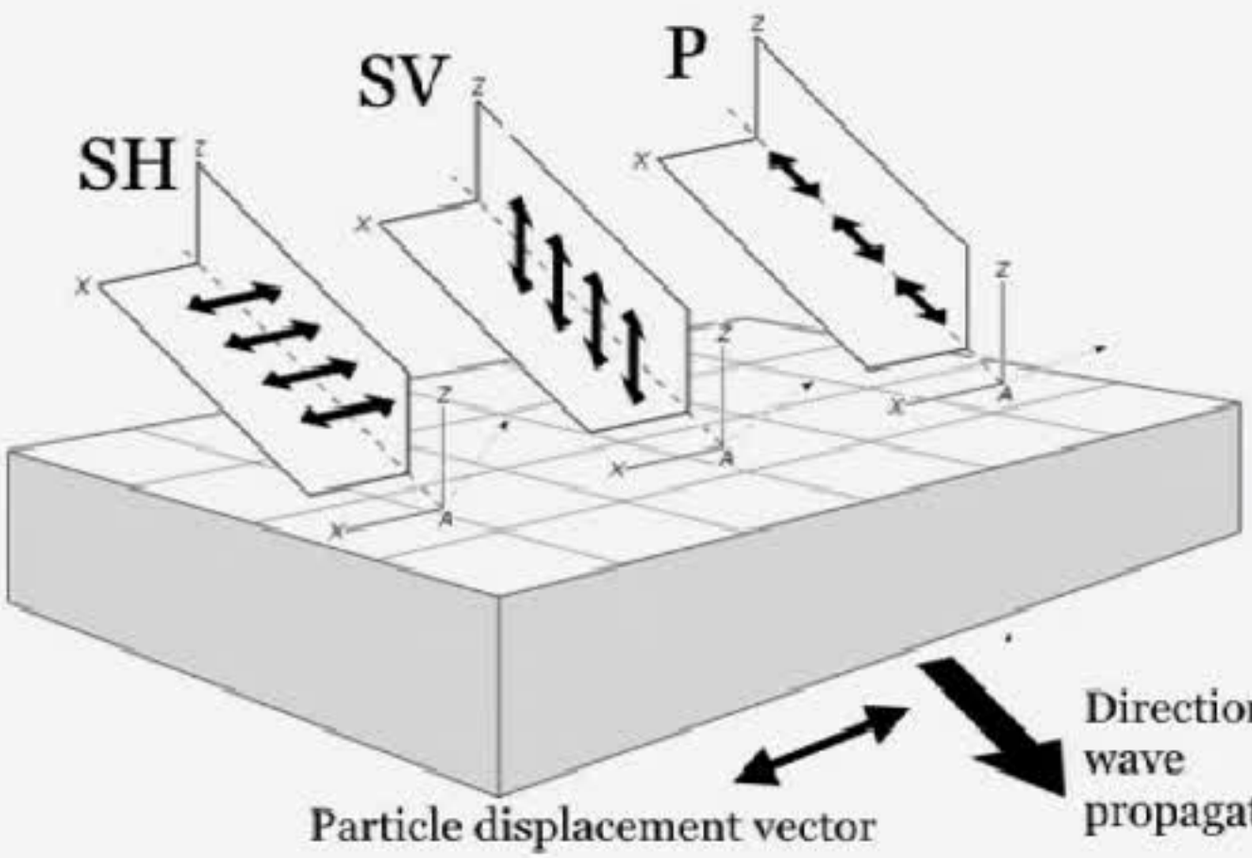

The seismic wavefield that propagates through the (isotropic) Earth consists of a P-wave component and two shear (SV and SH) wave components; their characteristic speed is respectively

$$c_P = \sqrt{\frac{\lambda + 2\mu}{\rho}}, \qquad c_S = \sqrt{\frac{\mu}{\rho}},$$

Weak form

For any time $t \in (0, T]$ find $\mathbf{u} \in \mathbf{V} = \mathbf{H}^1(\Omega)/\mathbb{R}$ such that

$$(\rho\ddot{\mathbf{u}}, \mathbf{v})_\Omega + \mathcal{A}(\mathbf{u}, \mathbf{v}) + (G(\mathbf{u}), \mathbf{v})_\Omega = \mathcal{F}(\mathbf{v}) \quad \forall \mathbf{v} \in \mathbf{V}$$

supplemented with initial conditions $\mathbf{u}(0) = \mathbf{u}^0$ and $\dot{\mathbf{u}}(0) = \mathbf{v}^0$

$$\mathcal{A}(\mathbf{u}, \mathbf{v}) = (\underline{\sigma}(\mathbf{u}), \underline{\varepsilon}(\mathbf{v}))_\Omega \qquad \mathcal{F}(\mathbf{v}) = (\mathbf{f}, \mathbf{v})_\Omega + \langle \mathbf{t}, \mathbf{v} \rangle_{\Gamma_N}$$

Up to "non-reflecting BCs terms"

Requirements on the numerical solution

- Accurate description of the behaviour at material interfaces
  ⇨ high-order accuracy
- Waves are typically propagated over many periods of time
  ⇨ control the numerical dispersion and dissipation errors
- Complex geometries and strong contrasts in wave speeds
  ⇨ methods that accommodate non-conforming grids
- The size of the bodies excited is large relative to the wavelengths of interests
  ⇨ efficient and scalable implementation for parallel computing

Discontinuous Galerkin Spectral Element methods (DGSEM)

Mesh partition

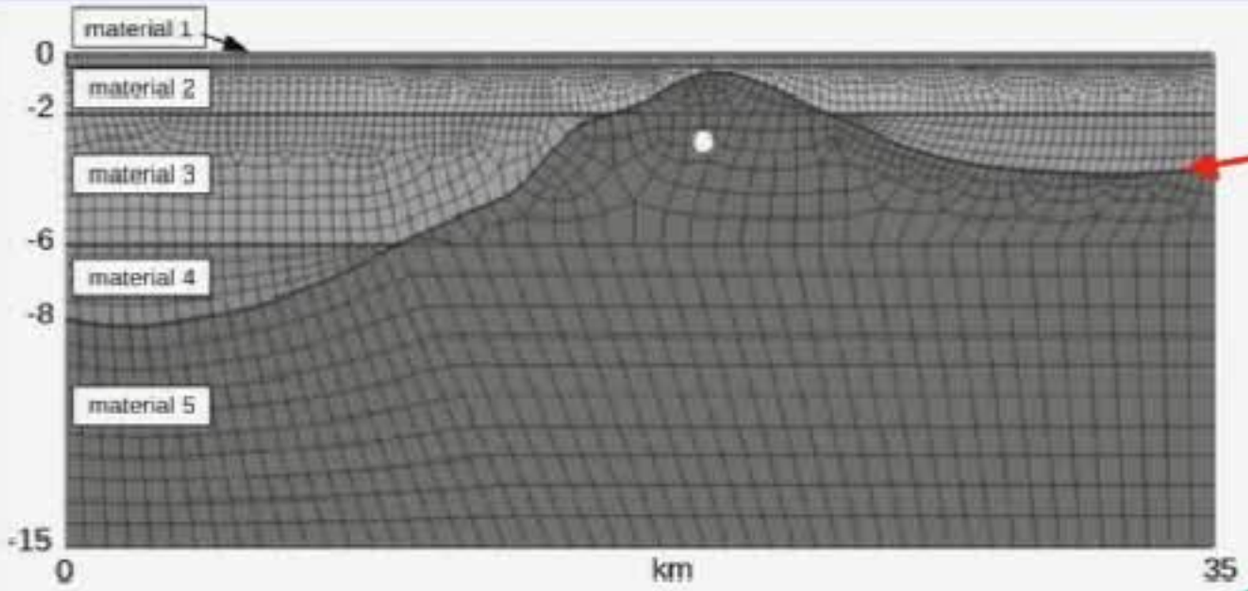

"DG faces" $\mathcal{F}_h$

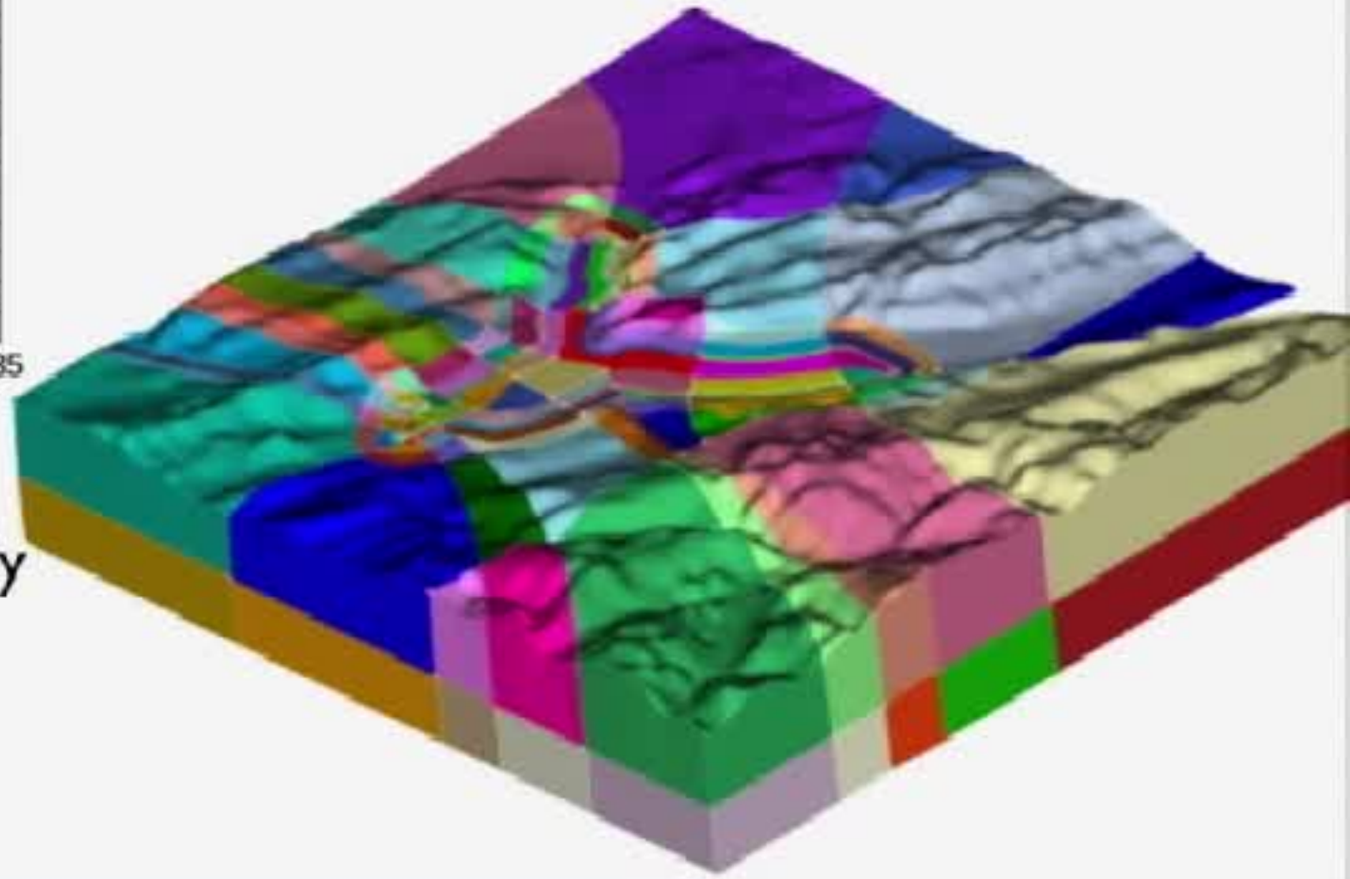

Ω is partitioned into macro-regions Ω_ℓ

Each macro-region is meshed independently by a conforming hexahedral/tetrahedral partition $\mathcal{T}_{h\ell}$

DG paradigm used at interfaces

A function in V_{DG} is

a polynomial of degree $N_\ell \geq 1$ in each mesh-element of $\mathcal{T}_{h\ell}$,

continuous in each macro-region,

discontinuous across the skeleton

Continuous in time approximation

For any time $t \in (0, T]$ find $\mathbf{u}_h \in \mathbf{V}_h$ such that

$$(\rho \ddot{\mathbf{u}}_h, \mathbf{v}_h)_\Omega + \mathcal{A}_h(\mathbf{u}_h \mathbf{v}_h) + (G(\mathbf{u}_h), \mathbf{v}_h)_\Omega = \mathcal{F}_h(\mathbf{v}_h) \quad \forall \mathbf{v}_h \in \mathbf{V}_h$$

supplemented with initial conditions $\mathbf{u}_h(0) = \mathbf{u}_h^0$ and $\dot{\mathbf{u}}_h(0) = \mathbf{v}_h^0$

$$\mathcal{A}_h(\mathbf{u}_h, \mathbf{v}_h) = \sum_{\Omega_\ell} (\underline{\sigma}(\mathbf{u}_h), \underline{\varepsilon}(\mathbf{v}_h))_{\Omega_\ell} + \langle \{\!\{\underline{\sigma}(\mathbf{u}_h)\}\!\}, [\![\mathbf{v}_h]\!] \rangle_{\mathcal{F}_h}$$

$$+ \langle [\![\mathbf{u}_h]\!], \{\!\{\underline{\sigma}(\mathbf{v}_h)\}\!\} \rangle_{\mathcal{F}_h} + \langle \eta [\![\mathbf{u}_h]\!], [\![\mathbf{v}_h]\!] \rangle_{\mathcal{F}_h}$$

Jump

Average

$$\mathcal{F}_h(\mathbf{v}_h) = \sum_{\Omega_\ell} (\mathbf{f}, \mathbf{v}_h)_{\Omega_\ell} + \langle \mathbf{t}, \mathbf{v}_h \rangle_{\mathcal{F}_h^N}$$

$$\eta \approx \alpha \{\!\{\mathbb{D}\}\!\} \left\{\!\!\left\{ \frac{N_\ell^2}{h_\ell} \right\}\!\!\right\}$$

α large enough

Stability

Let $\mathbf{u}_h(t)$ be the continuous in time approximate solution (with $\mathbf{t} = \mathbf{0}$, for simplicity). Then

$$\|\mathbf{u}_h(t)\|_{\mathcal{E}}^2 \lesssim \|\mathbf{u}_h(0)\|_{\mathcal{E}}^2 + \int_0^t \rho_*^{-1} \|\mathbf{f}(\tau)\|_{L^2(\Omega)} \, d\tau \quad 0 < t \leq T$$

$$\|\mathbf{v}(t)\|_{\mathcal{E}}^2 = \|\rho^{1/2}\dot{\mathbf{v}}(t)\|_{L^2(\Omega)}^2 + \|\rho^{1/2}\zeta\mathbf{v}(t)\|_{L^2(\Omega)}^2 + \sum_{\ell} \|\underline{\mathbb{D}}^{1/2}\underline{\varepsilon}(\mathbf{v}(t))\|_{L^2(\Omega_\ell)}^2 + \|\eta^{1/2}\,[\![\mathbf{v}(t)]\!]\,\|_{L^2(\mathcal{F}_h)}^2$$

[Antonietti, Ayuso, Mazzieri, Quarteroni, JSC, 2016],[Antonietti, Ferroni, Mazzieri, Quarteroni, LNCES, 2017], [Antonietti, Mazzieri, CMAME, 2018]

Error estimates

$$\sup_{t\in[0,T]} \|\mathbf{u}(t) - \mathbf{u}_h(t)\|_{\mathcal{E}}^2 \lesssim \sum_{\Omega_\ell} C_\ell(T, \mathbf{u}, \dot{\mathbf{u}}, \ddot{\mathbf{u}}) \frac{h_\ell^{2\min(s_\ell, N_\ell+1)-2}}{N_\ell^{2s_\ell-3}}$$

If $h_\ell \approx h$, $N_\ell = N$, and $s_\ell = s \geq N+1$ for any $\ell = 1, 2, \ldots$

$$\sup_{t\in[0,T]} \|\mathbf{u}(t) - \mathbf{u}_h(t)\|_{\mathcal{E}}^2 \lesssim C(T, \mathbf{u}, \dot{\mathbf{u}}, \ddot{\mathbf{u}}) \frac{h^{2N}}{N^{2s-3}}$$

- Large enough penalty parameter
- Optimal rate of convergence with respect to h
- Suboptimal (by a factor $N^{1/2}$) rate of convergence with respect to N (known for DG methods)

Fully discrete formulation

$$\mathsf{M}\ddot{\mathsf{U}}(t) + \mathsf{C}\dot{\mathsf{U}}(t) + \mathsf{A}\mathsf{U}(t) = \mathsf{F}(t),$$

$\mathsf{U}(0) = 0$ and $\dot{\mathsf{U}}(0) = 0$.

leapfrog $\longrightarrow$

$$\ddot{\mathsf{U}}(t_n) \approx \frac{\mathsf{U}^{n+1} - 2\mathsf{U}^n + \mathsf{U}^{n-1}}{\Delta t^2}, \qquad \dot{\mathsf{U}}(t_n) \approx \frac{\mathsf{U}^{n+1} - \mathsf{U}^{n-1}}{2\Delta t}$$

$$\left(\mathsf{M} + \frac{\Delta t}{2}\mathsf{C}\right)\mathsf{U}^{n+1} = \Delta t^2(\mathsf{F}^n - \mathsf{A}\mathsf{U}^n) + 2\mathsf{M}\mathsf{U}^n + \left(\frac{\Delta t}{2}\mathsf{C} - \mathsf{M}\right)\mathsf{U}^{n-1}, \quad n = 1, ..., N_T - 1$$

Newmark $\longrightarrow$

$$\mathsf{B}(t) = \mathsf{M}^{-1}(\mathsf{F}(t) - \mathsf{C}\dot{\mathsf{U}}(t) - \mathsf{A}\mathsf{U}(t))$$

$$\begin{cases} \mathsf{U}^{n+1} = \mathsf{U}^n + \Delta t\dot{\mathsf{U}}^n + \Delta t^2\left[\xi\mathsf{B}^{n+1} + (1/2 - \xi)\mathsf{B}^n\right] \\ \dot{\mathsf{U}}^{n+1} = \dot{\mathsf{U}}^n + \Delta t\left[\theta\mathsf{B}^{n+1} + (1 - \theta)\mathsf{B}^n\right] \end{cases}$$

$n = 1, ..., N_T - 1$

Adaptive time-integration methods (see conclusions)

Verification: layer over halfspace

- $\Omega = [-30, 30] \times [-30, 30] \times [0, 17]$ km
- Seismic moment in $S = (0, 0, 2)$ km ★
- Receiver $R = (6, 8, 0)$ km ●

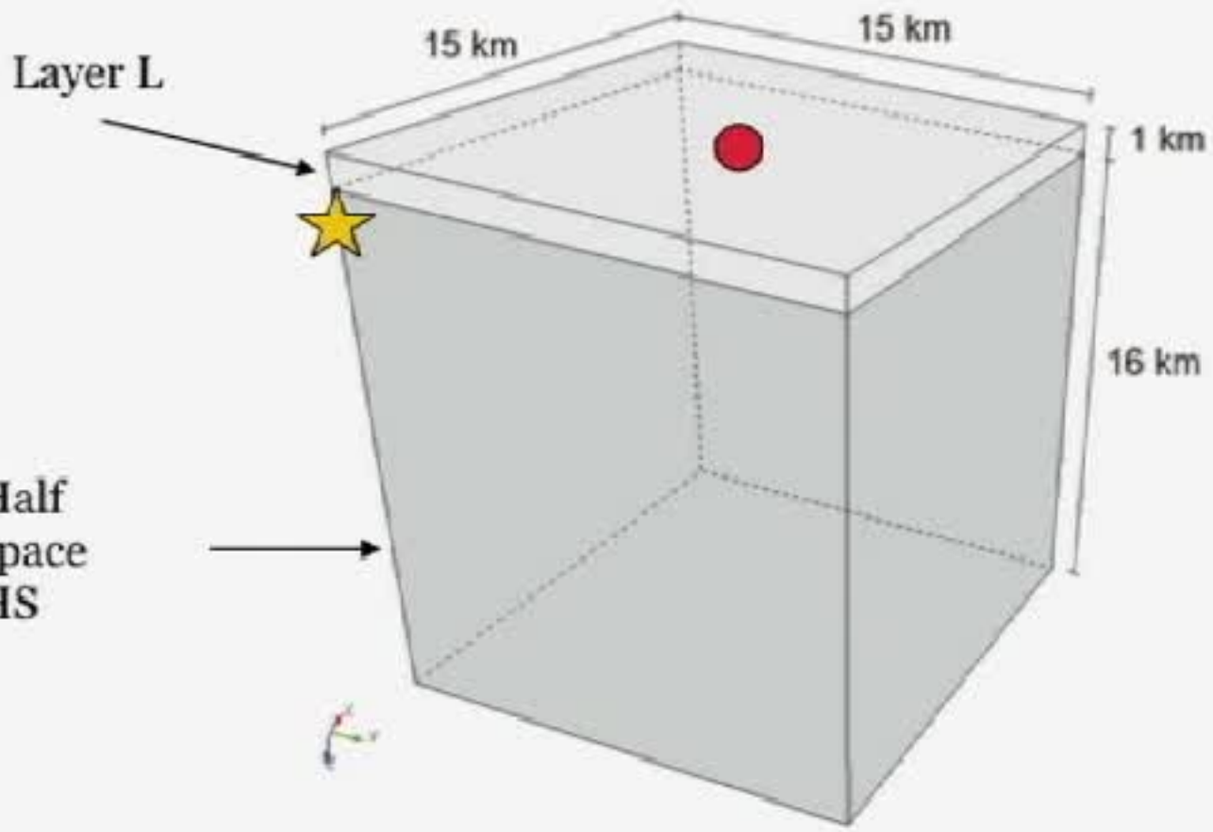

1 of 4 symmetric quadrants

$$\mathbf{f}(\mathbf{x}, t) = -\nabla \cdot \delta(\mathbf{x} - \mathbf{x}_S) g(t)$$

$$g(t) = M_0 \left(t/t_0^2\right) \exp\left(-t/t_0\right)$$

$$M_0 = 10^8 \ [Nm]$$

$$t_0 = 0.1 \ [s]$$

Moment time history

Layer	Depth $[m]$	$c_P[m/s]$	$c_S[m/s]$	$\rho[kg/m^3]$
L	0-1000	4000	2000	2600
HS	1000-17000	6000	3464	2700

[Day et al. Bulletin of the Seismological Society of America 2001]

Verification: layer over halfspace

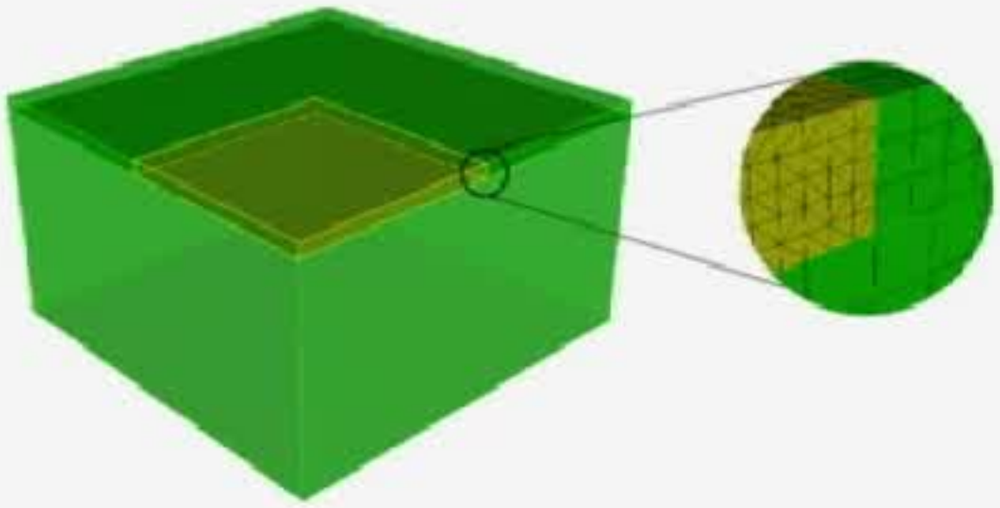

Model	El.	N	d.o.f.	Δt
Hexa-C	814833	4	≈150 mln	$3 \cdot 10^{-4}$
Hexa-NC	70228	5	≈30 mln	$5 \cdot 10^{-4}$
Hexa-Tetra	86141	5-4	≈30 mln	$5 \cdot 10^{-4}$

Relative seismogram misfit

$$E = \frac{\sum_{i=1}^{N_T} (\mathbf{u}_h(t_i) - \mathbf{u}(t_i))^2}{\sum_{i=1}^{N_T} \mathbf{u}(t_i)^2}$$

Hexa-C provide same results as Hexa-NC

[Mazzieri, Stupazzini, ,Guidotti, Smerzini, Int. J. Numer. Meth. Eng., 2013]

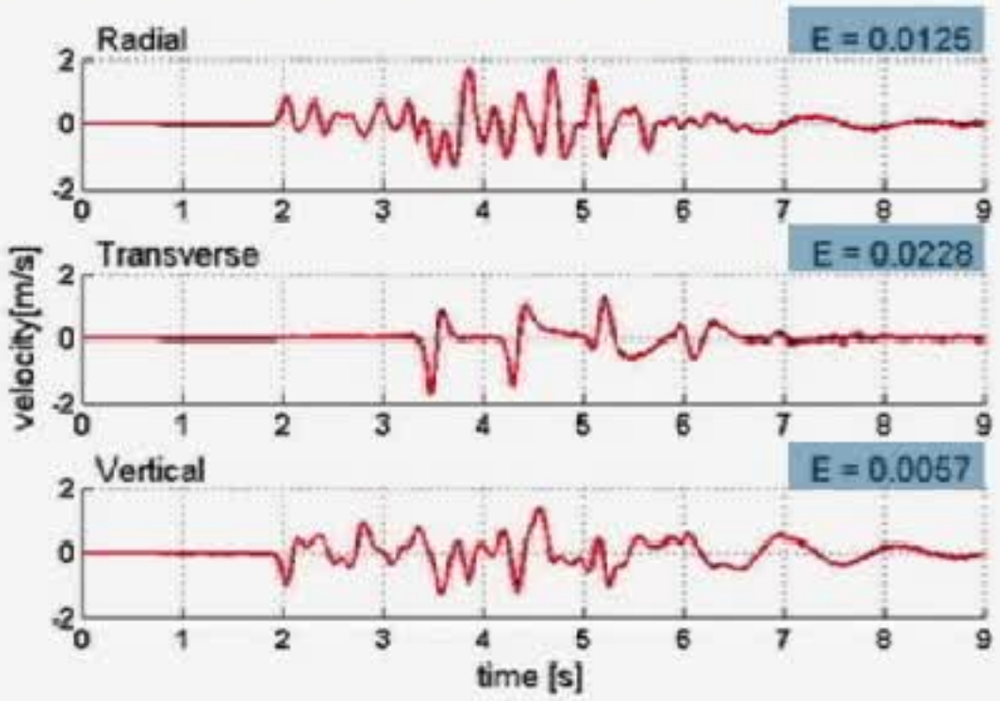

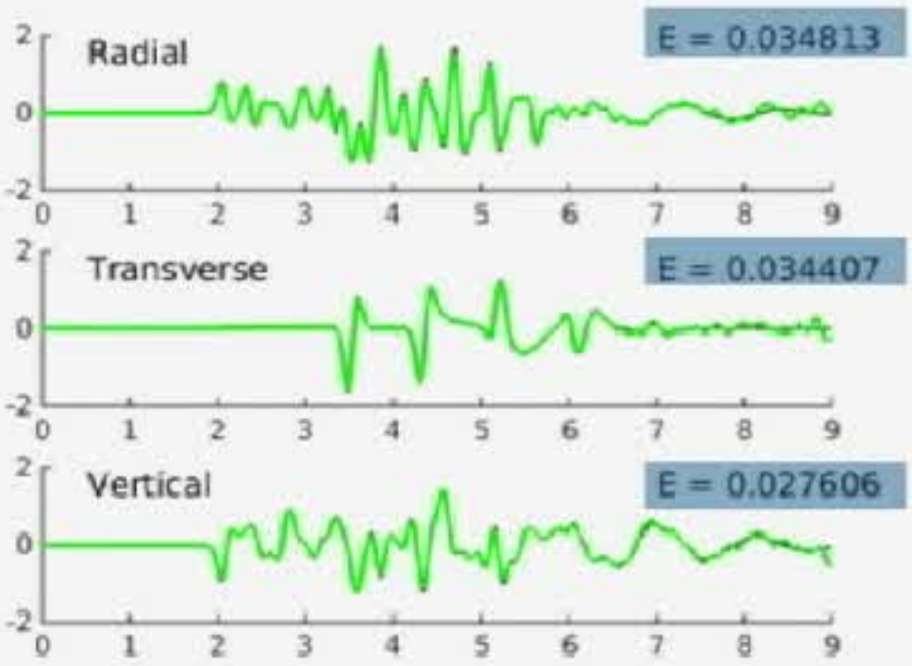

Comparison between the semi-analytic solution (black line) and the numerical one (colored line)

3D Grid dispersion and dissipation: plane wave analysis

In an infinite elastic medium free from body forces, the displacement field is governed by the equation

$$\rho \ddot{\mathbf{u}} - \nabla \cdot \underline{\sigma}(\mathbf{u}) = \mathbf{0}$$

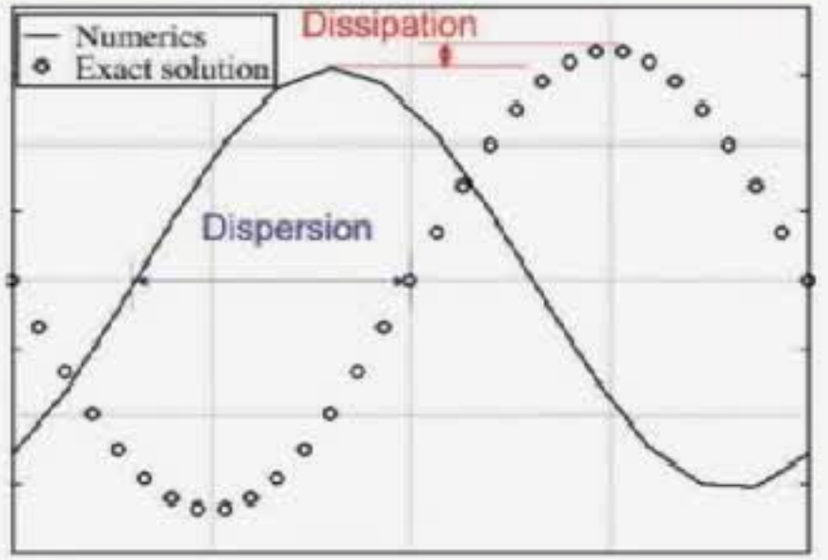

We seek the solution in the form of a plane wave:

$$\mathbf{u}(\mathbf{x}, t) = \mathbf{A} e^{i(\mathbf{k}\cdot\mathbf{x} - \omega t)}$$

$\mathbf{A} = [A_1, A_2, A_3]^T$: the amplitude of the wave

ω: the angular frequency

$\mathbf{k} = 2\pi/L(\cos\theta\cos\phi, \sin\theta\cos\phi, \sin\phi)$ the wavenumber vector

L: wavelength

θ and ϕ : angles between the direction of propagation and the coordinate axes

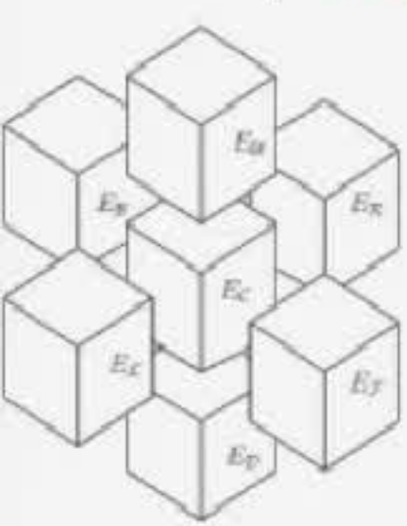

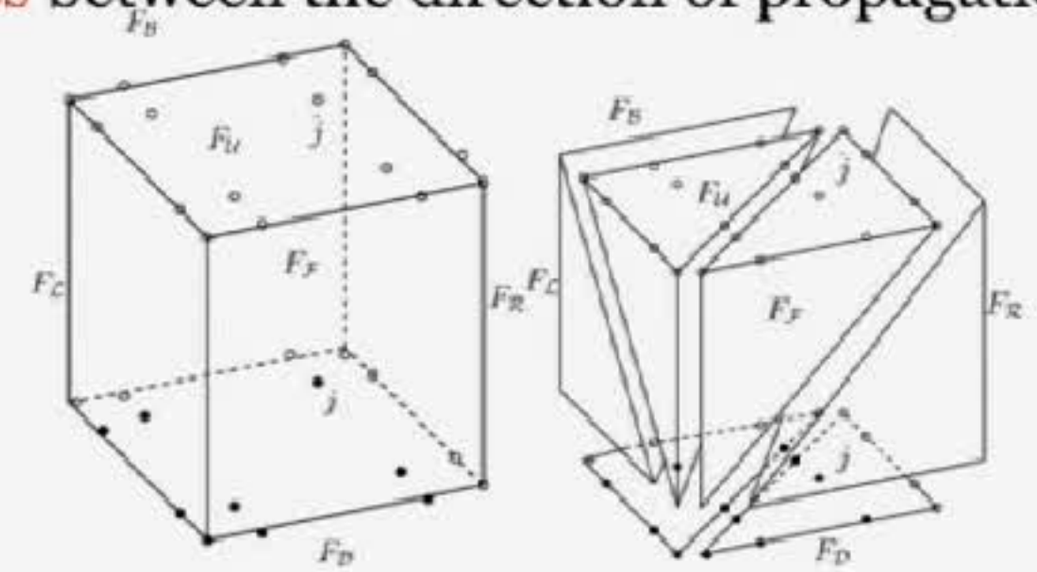

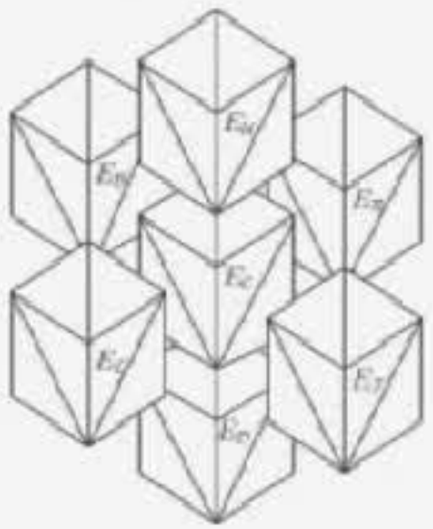

Periodic tessellation based on employing hex/tet grids

[De Basabe et al., Geophys. J. Int. 2010], [Ainsworth et al, J. Sci. Comput. 2006] [Seriani et al. Wave Motion, 2008], [Ferroni, Antonietti, Mazzieri, Quarteroni, Geophys. J. Int. 2017]

3D Grid dispersion analysis (cont'd)

Relative dispersion errors

$$e_S = \frac{c_{S,h}}{c_S} - 1.$$

$c_S = \sqrt{\mu/\rho}$ speed of shear waves

$c_{S,h}$ ⟶ numerical wave velocity

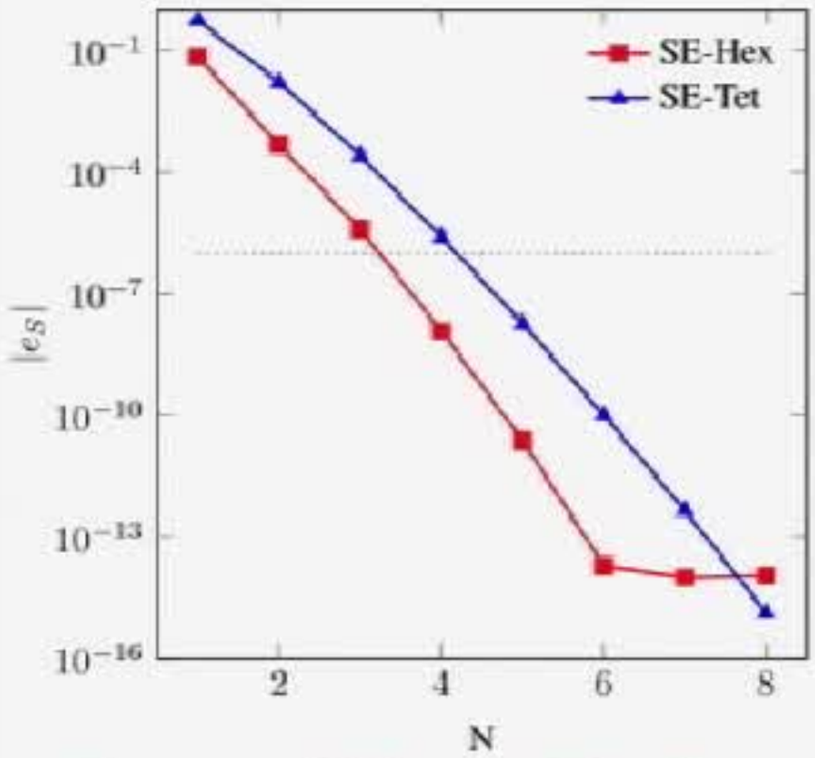

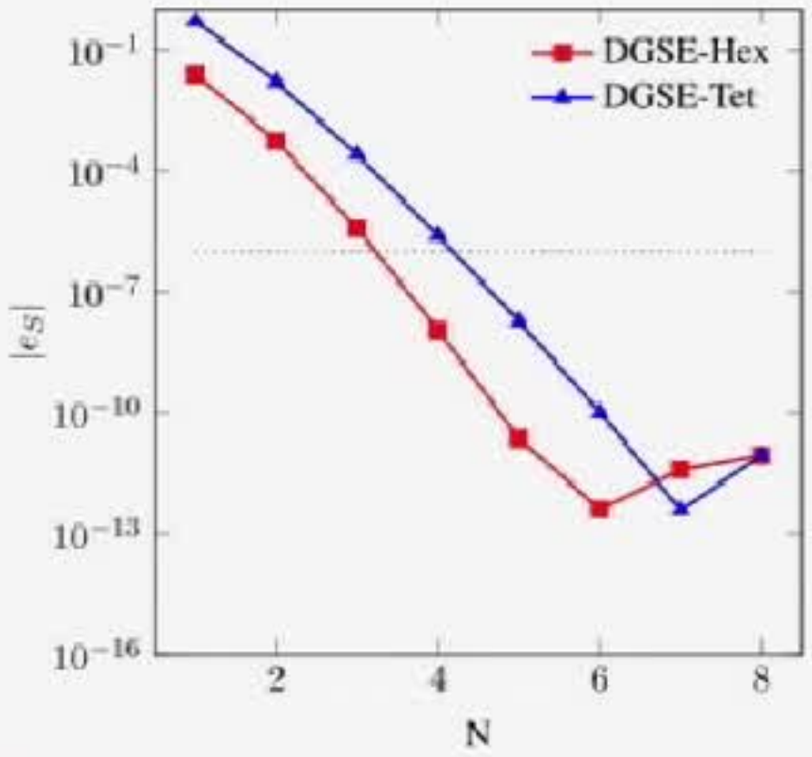

Computed dispersion errors $|e_S|$ versus N with

$\delta = 5$, $\theta = \phi = \pi/4$ and $r = 2$

Dotted line = threshold value 10^{-6}.

- Exponential decay of the dispersion error with respect to the polynomial degree N
- SE feature slightly low dispersion error compared to DGSE
- For both SE and DGSE approximations
  - on hexahedral grids negligible dispersion errors (i.e. less than 10^{-6}) can be achieved using a polynomial approximation degree $N \geq 4$
  - on tetrahedral grids negligible dispersion errors can be achieved using a polynomial approximation degree $N \geq 5$

[Ferroni, Antonietti, Mazzieri, Quarteroni, Geophys. J. Int. 2017]

Lesson learnt

- As far as you can, use continuous (conforming) SEM
- To treat faults and material discontinuities, DGSEM offer a very valuable alternative to continuous SEM
- Tetrahedral DGSEM are definitely easier to implement than tetrahedral continuous SEM when dealing with complex geometries

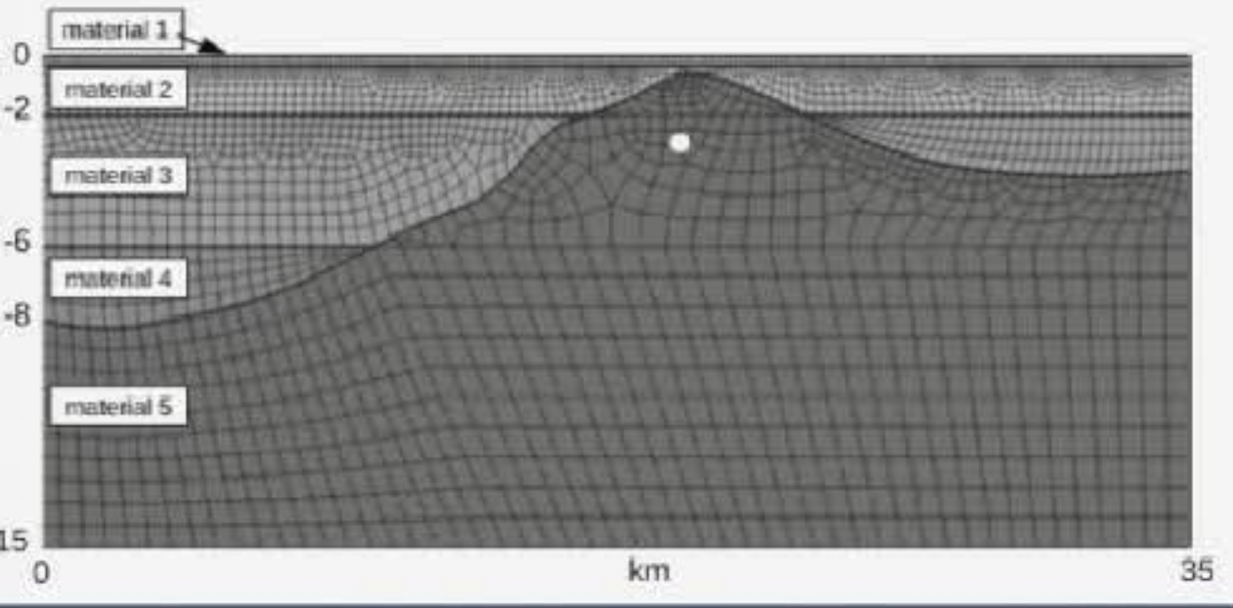

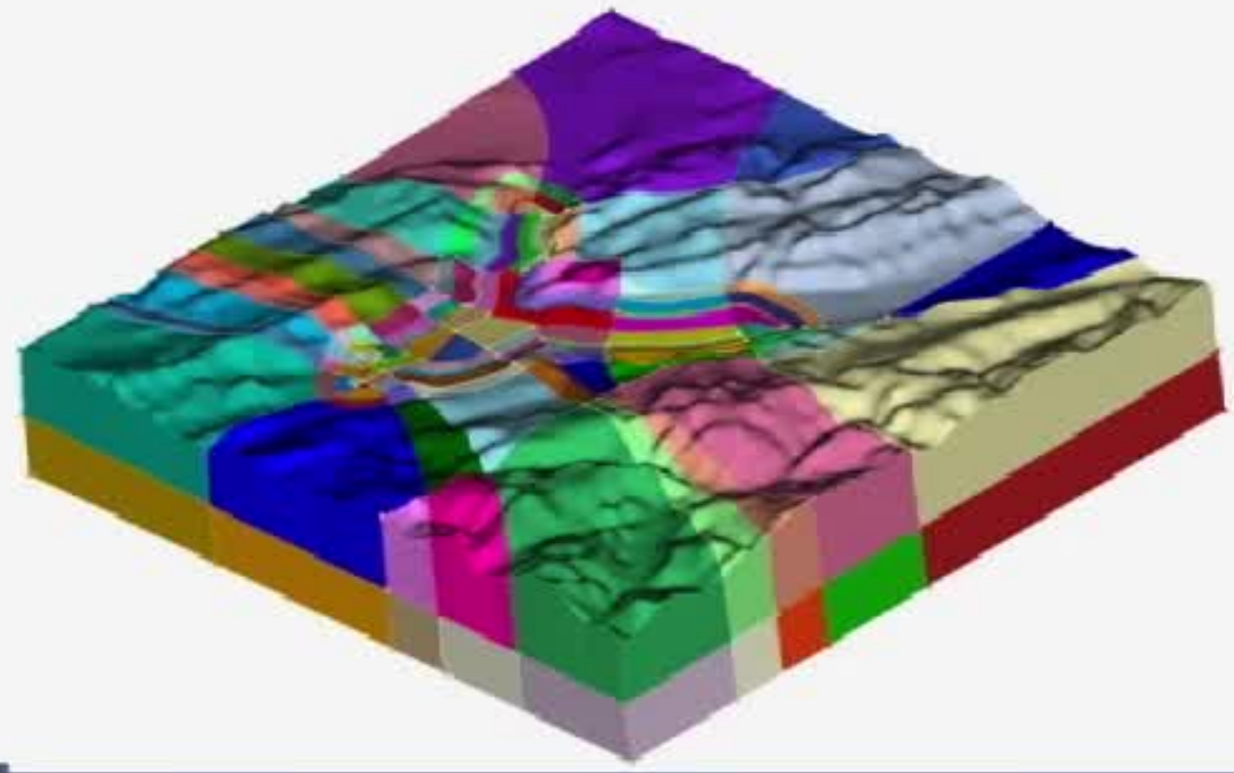

Emilia (IT) earthquake
29.05.2012, Mw 6.0

Courtesy of G. Penna

Emilia earthquake, 29.05.2012, M_W 6.0

Emilia earthquake, 29.05.2012, M_W 6.0

Emilia earthquake, 29.05.2012, M_W 6.0

Emilia earthquake, 29.05.2012, M_W 6.0

Emilia earthquake, 29.05.2012, M_W 6.0

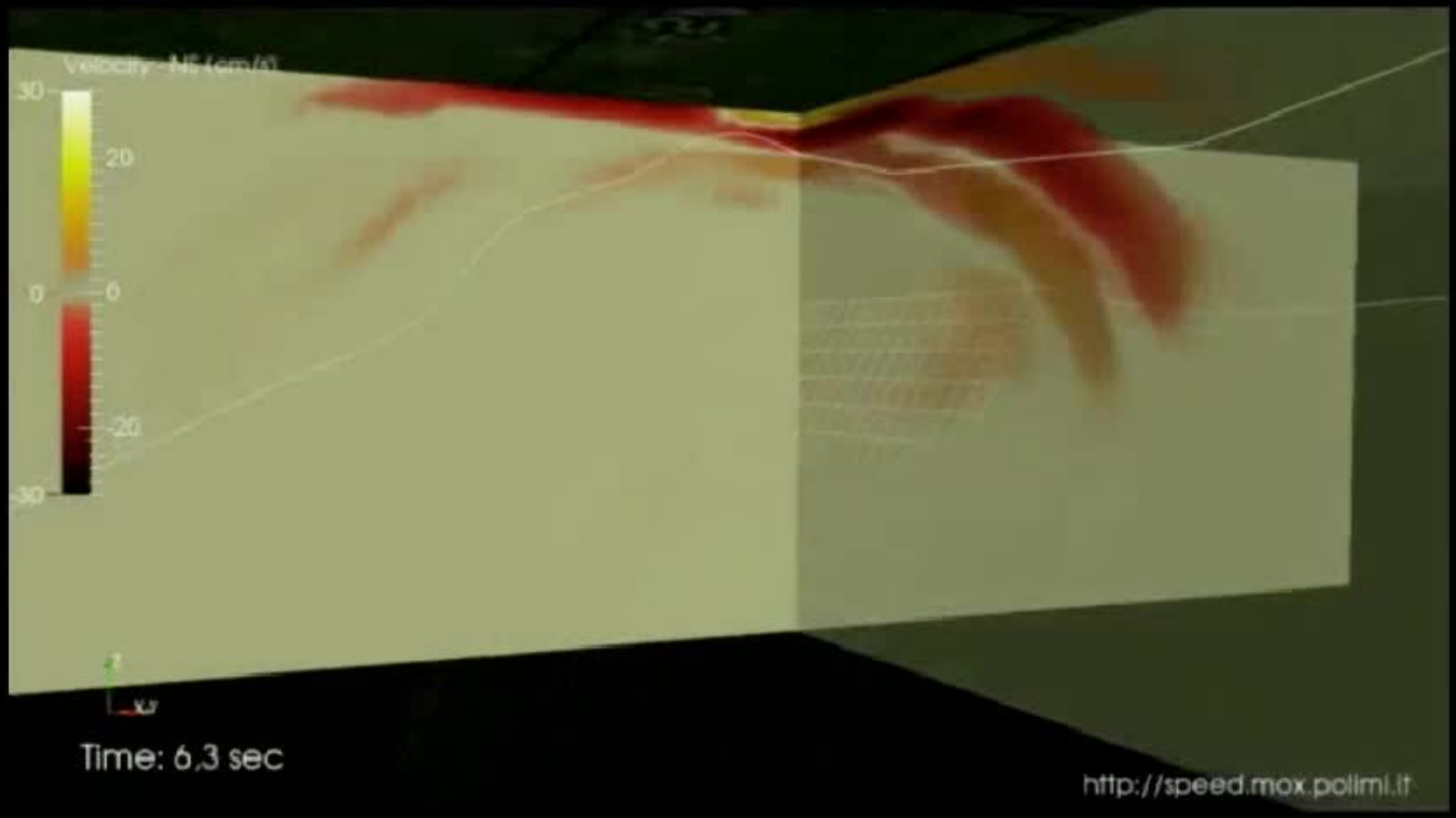

Emilia earthquake, 29.05.2012, M_W 6.0

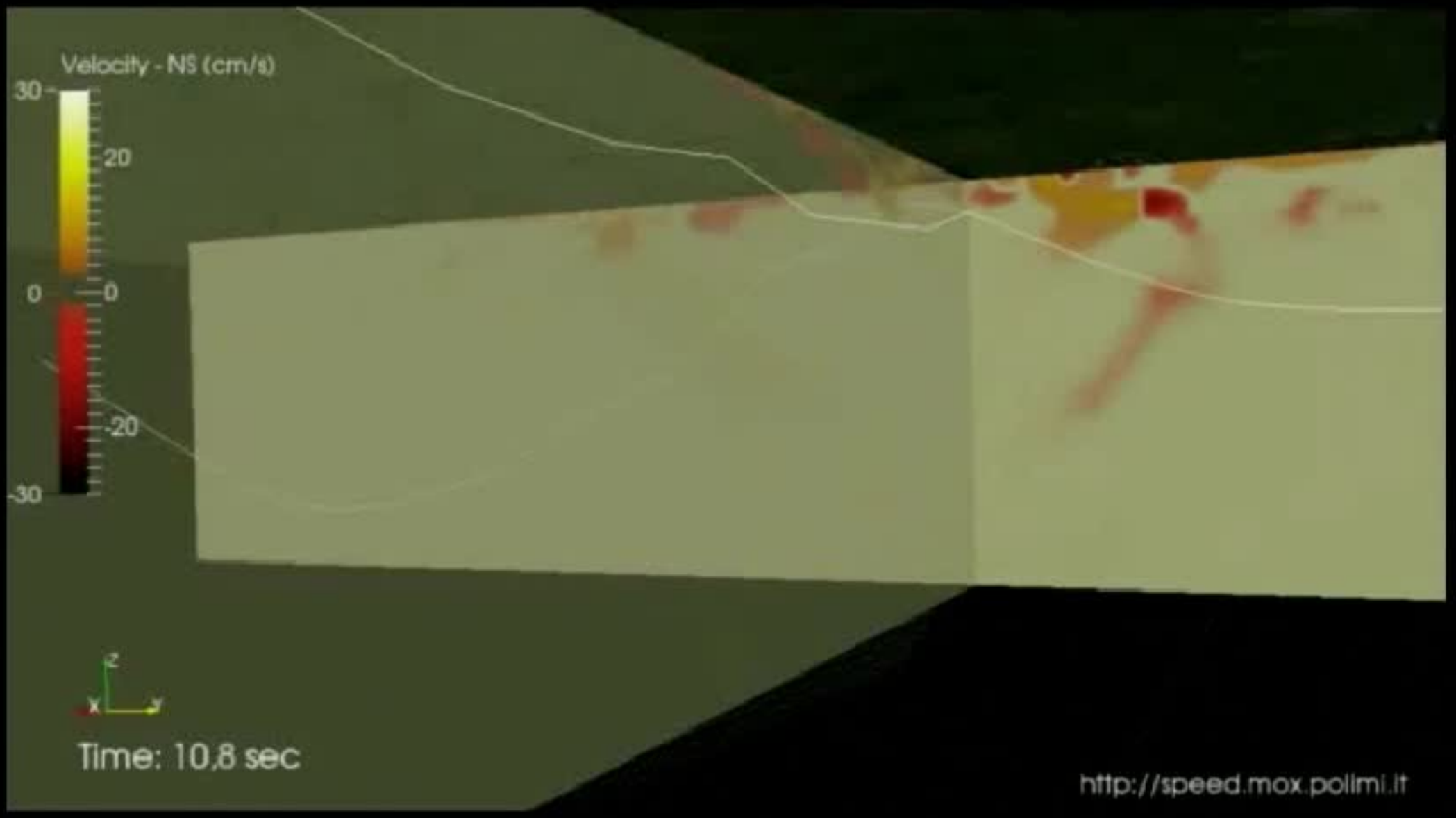

Set-up of the 3D model

- Kinematic seismic source for the Mirandola fault
- 3D velocity model of the Po Plain (Plio-Quaternary sediments)
- Linear visco-elastic model
- f_{max} = 1.5 Hz
- dofs ~ 150 million (polynomials of degree 3)
- T_{sim} ~ 5 hours on 4096 cores (Fermi@Cineca - ITALY)

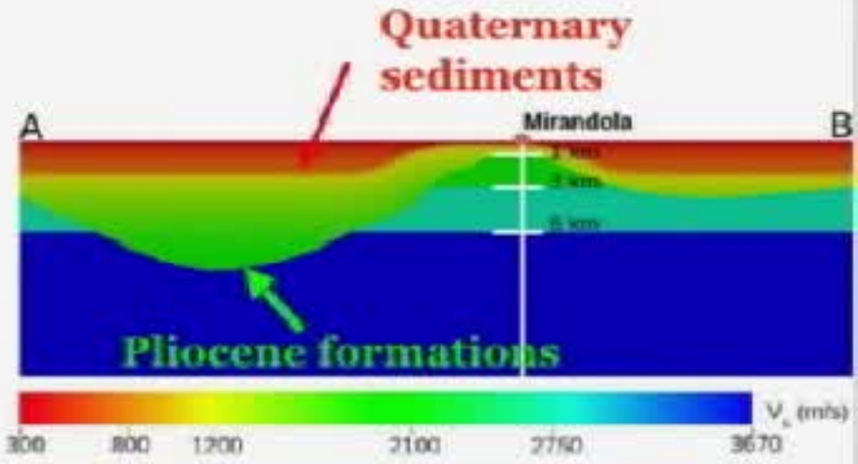

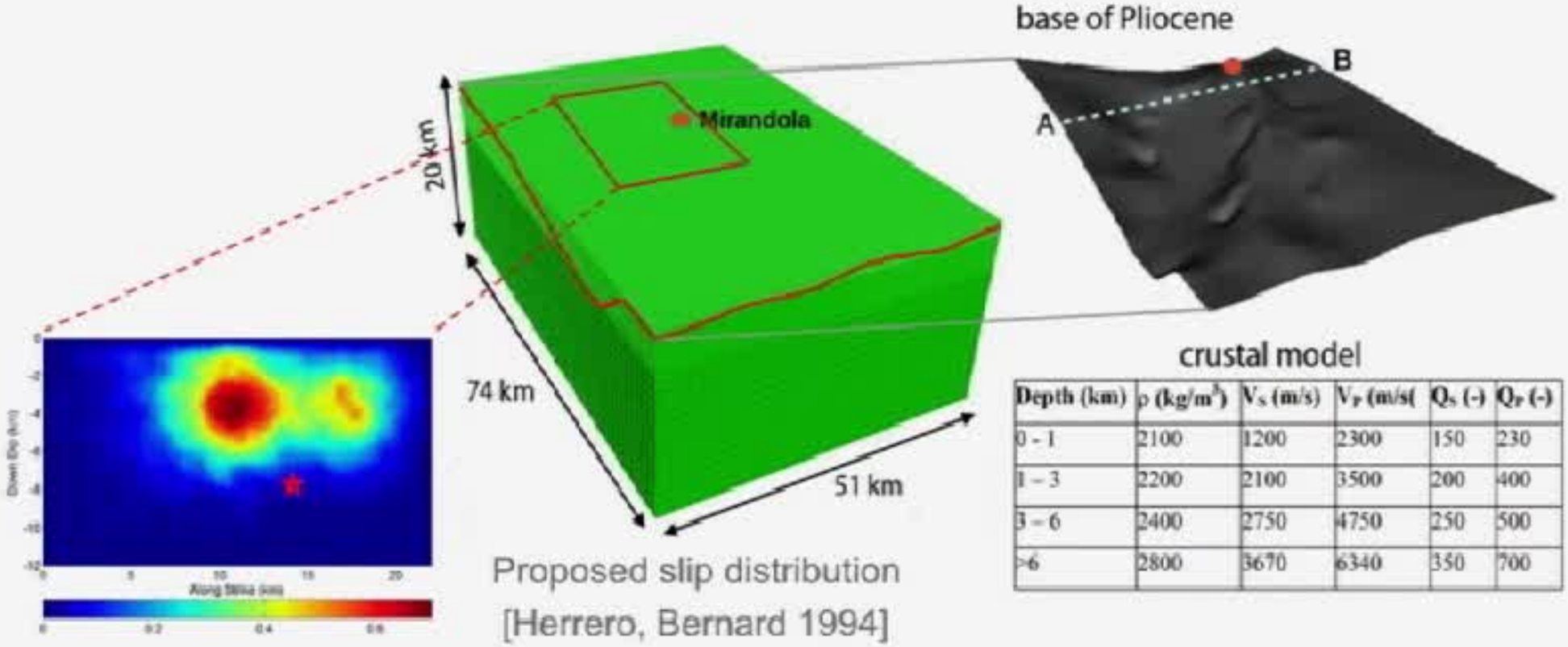

Proposed slip distribution
[Herrero, Bernard 1994]

crustal model

Depth (km)	ρ (kg/m^3)	V_S (m/s)	V_P (m/s(	Q_S (-)	Q_P (-)
0 - 1	2100	1200	2300	150	230
1 – 3	2200	2100	3500	200	400
3 – 6	2400	2750	4750	250	500
>6	2800	3670	6340	350	700

[Paolucci et al., JGI 2015]

Athens earthquake
September 7, 1999, Mw 6.0

Athens, Acropolis, Parthenon: elevation and topography

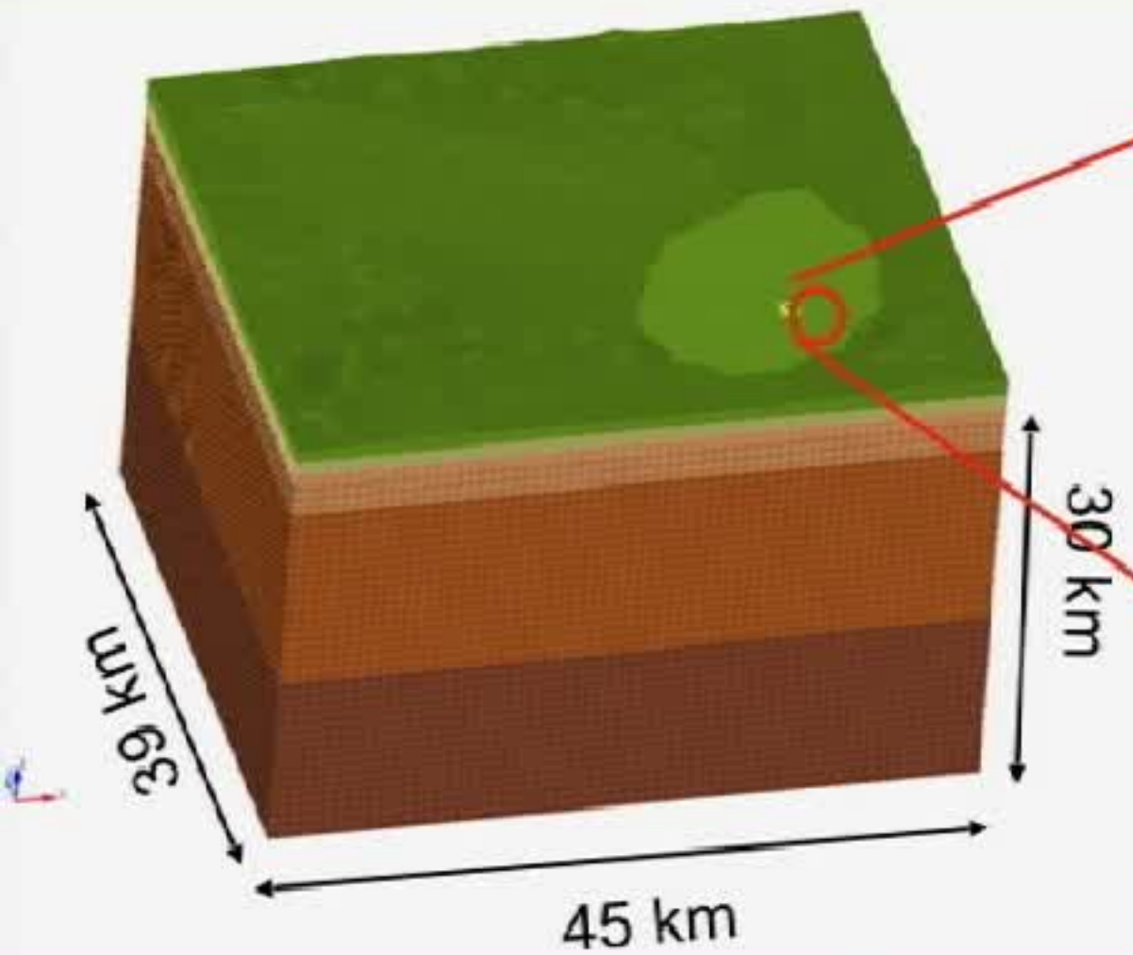

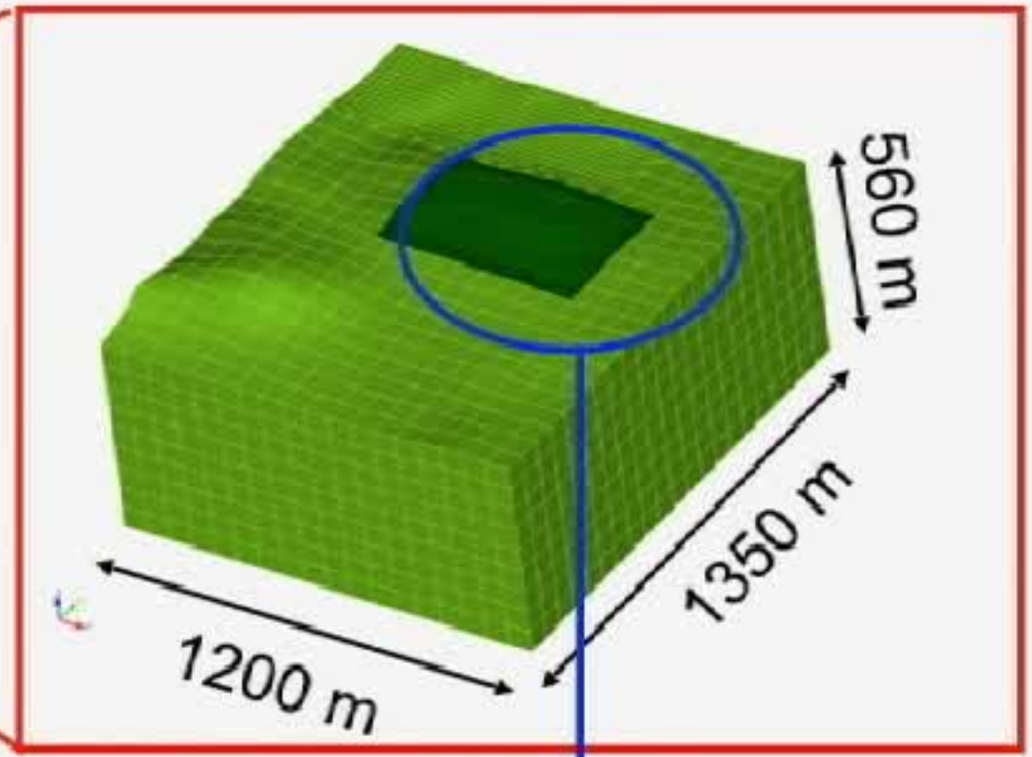

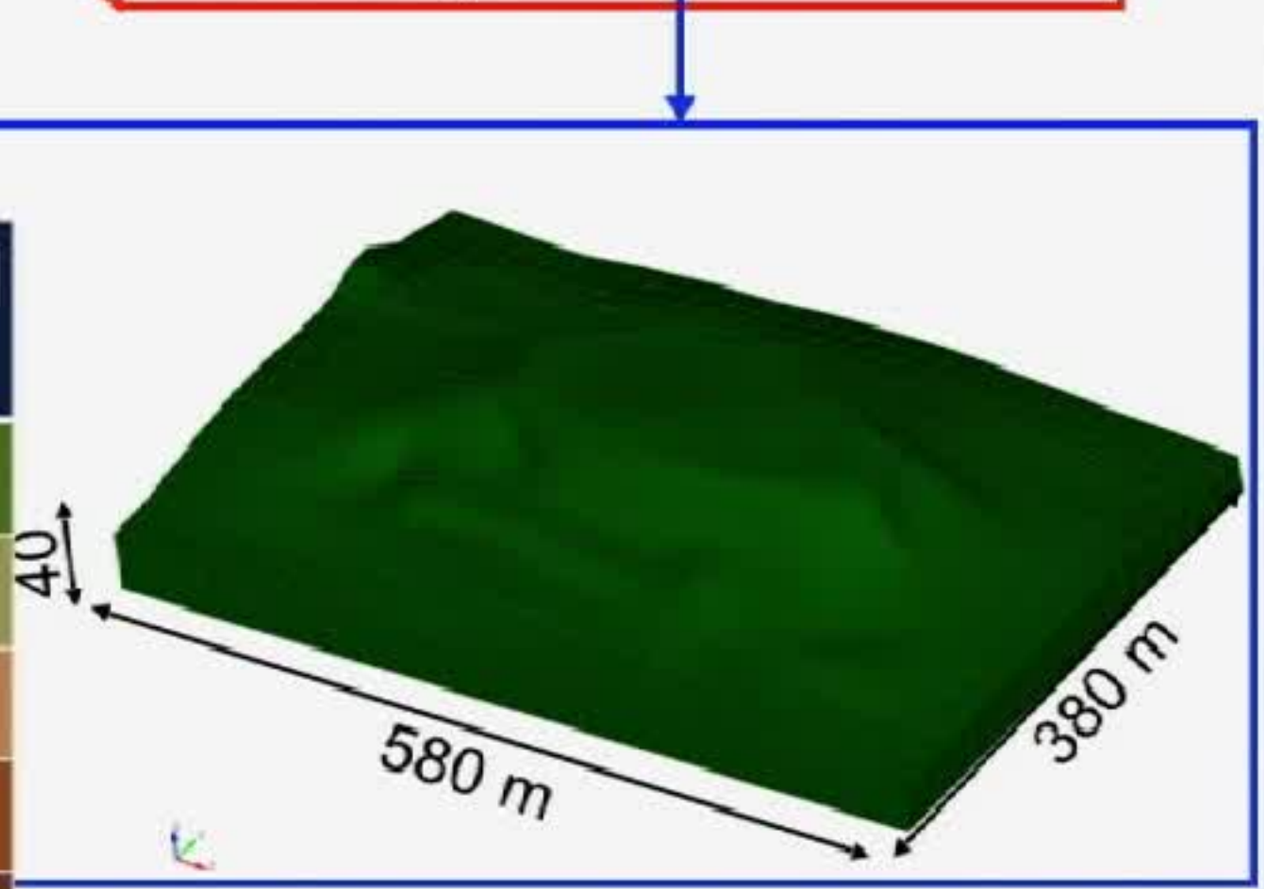

Bottom Depth [km]	C_p [m/s]	C_s [m/s]	[g/cm3]
Top – 1	2670	1500	2.50
1 – 2	4450	2500	2.50
2 – 5	5700	3200	2.84
5 – 18	6000	3370	2.90
18 – 30	6400	3600	2.98

Computational grid: Parthenon and Acropolis

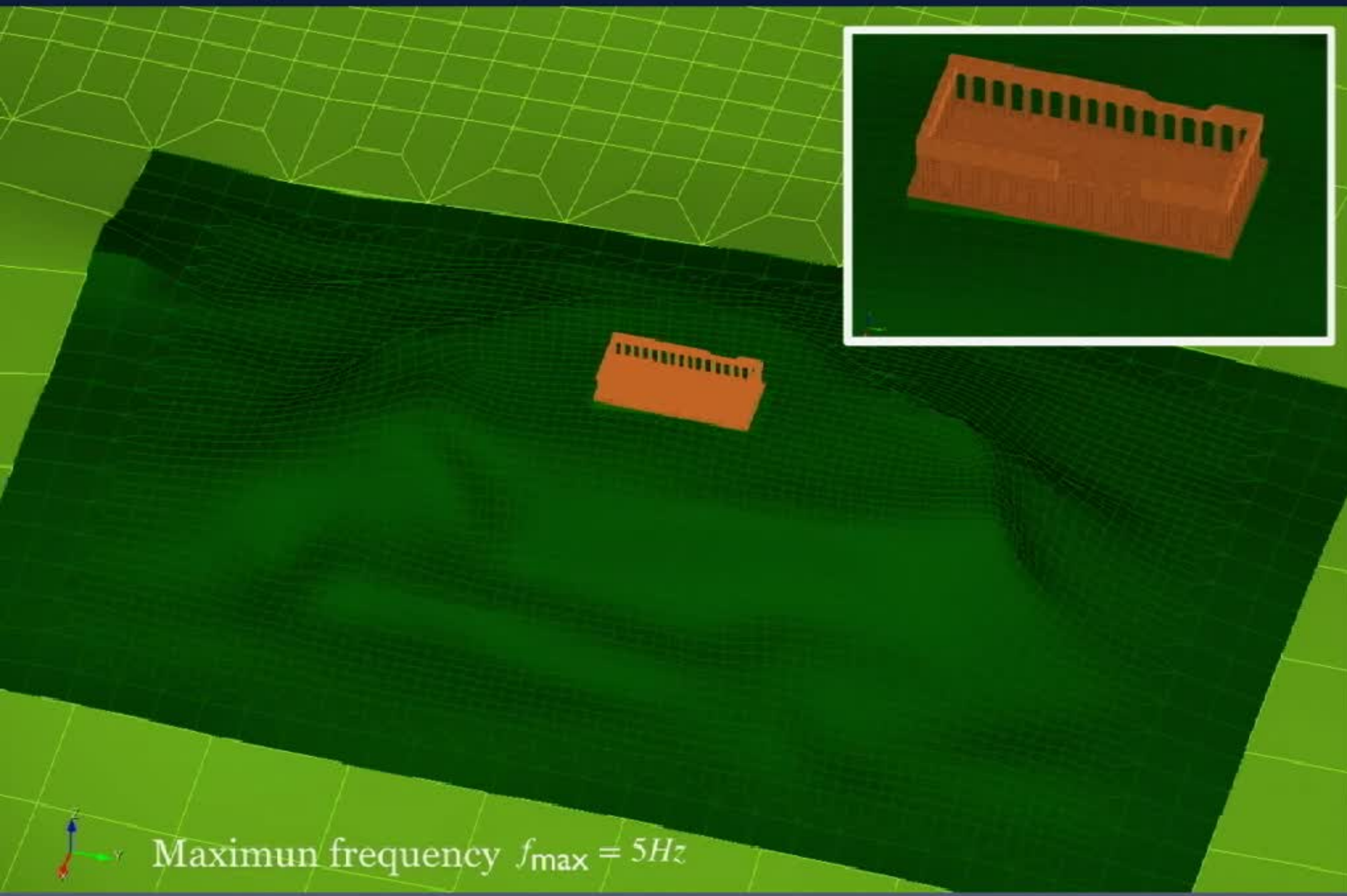

Computational model: mesh parameters

ID Block	N	h [m]
1	1	5 – 20
2	2	65
3	4	70 – 300
4	4	200 – 300
5	4	700
6	4	700
7	4	700

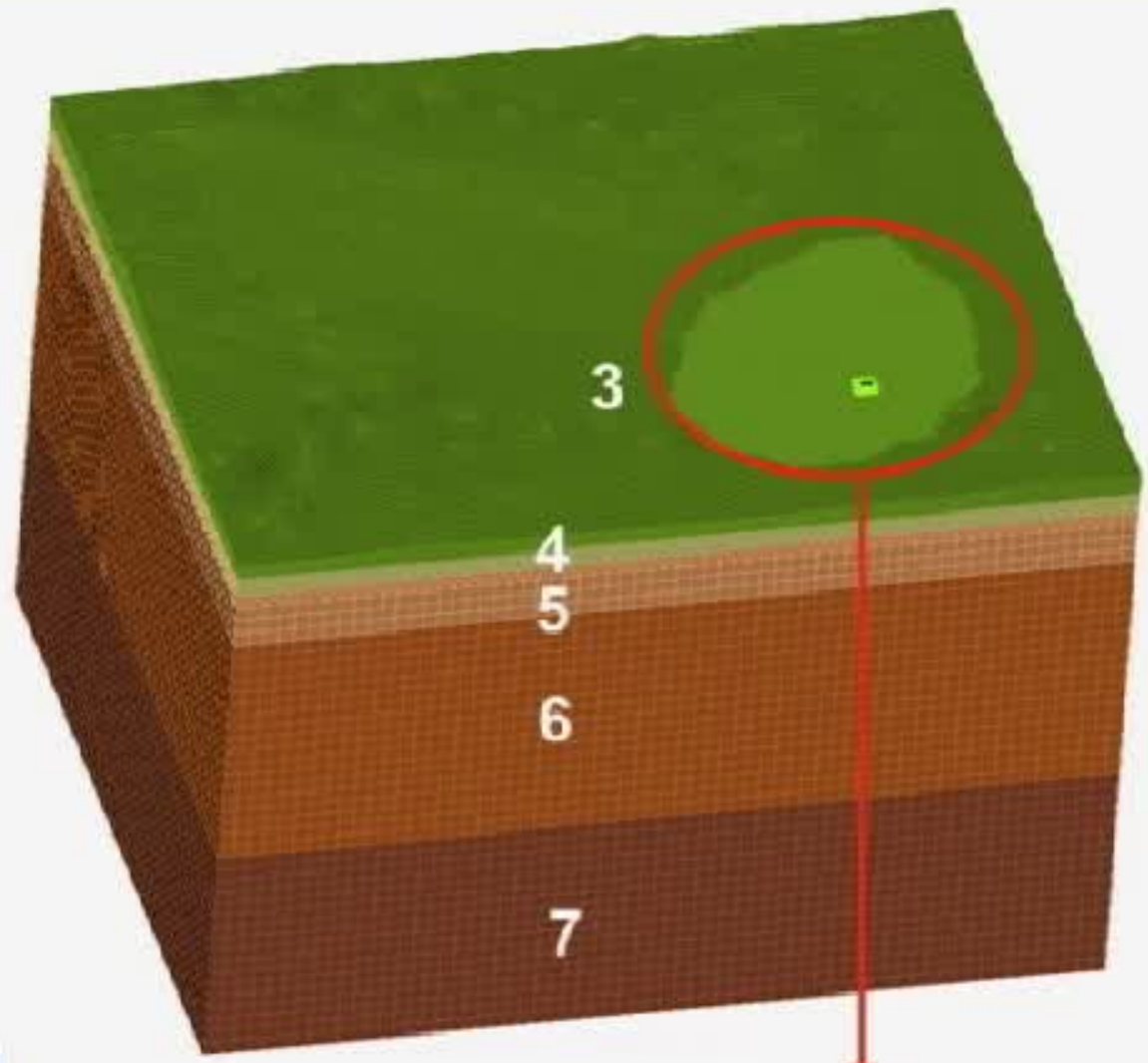

84 millions DOFS

$\Delta t = 10^{-4} s$

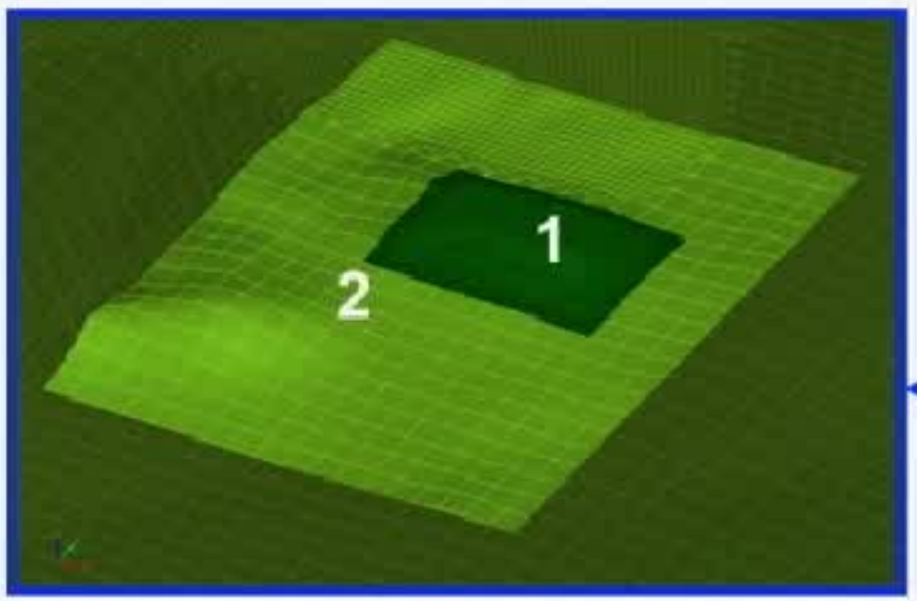

Computational model: the Parthenon

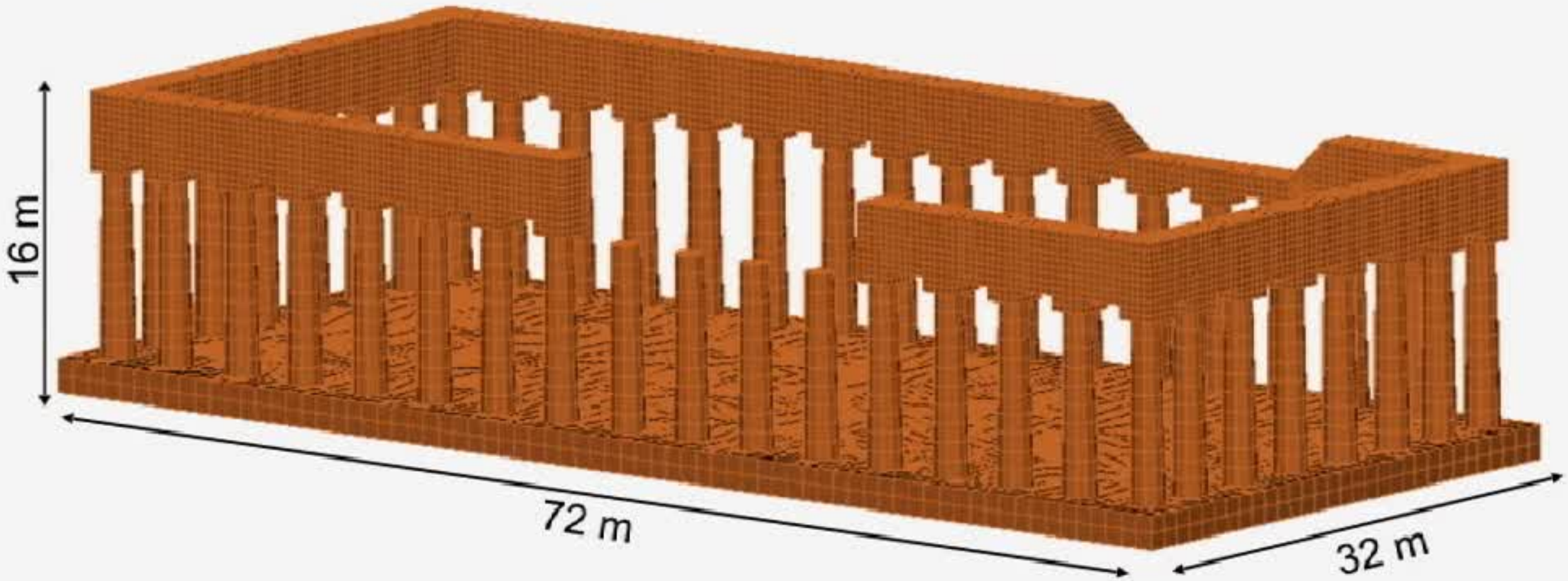

Material and mesh properties of the Parthenon

Material	C_p [m/s]	C_s [m/s]	ρ [g/cm3]	N	h [m]
Porous marble	1000	600	2.50	1	0.5

[Egglezos, Ioannidou, Moullou, Kalogeras, Geotechnics and Heritage: Case Histories, 2013]

Velocity magnitude snapshots

t = 4*s*

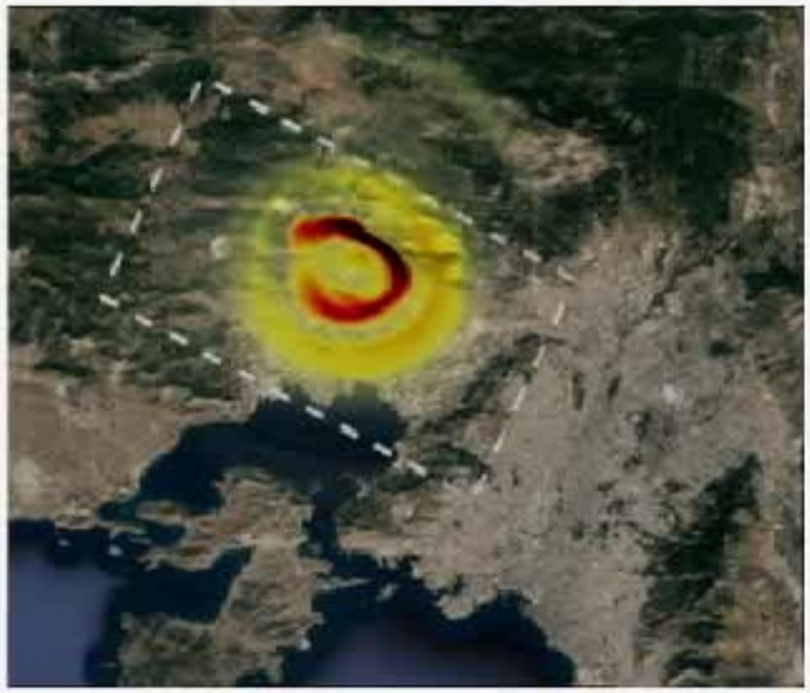

t = 5*s*

t = 6*s*

t = 8*s*

|v| (m/s)

Peak-ground velocity map

$$PGV = \sqrt{\max_t |v_x(t)| \max_t |v_y(t)|}$$

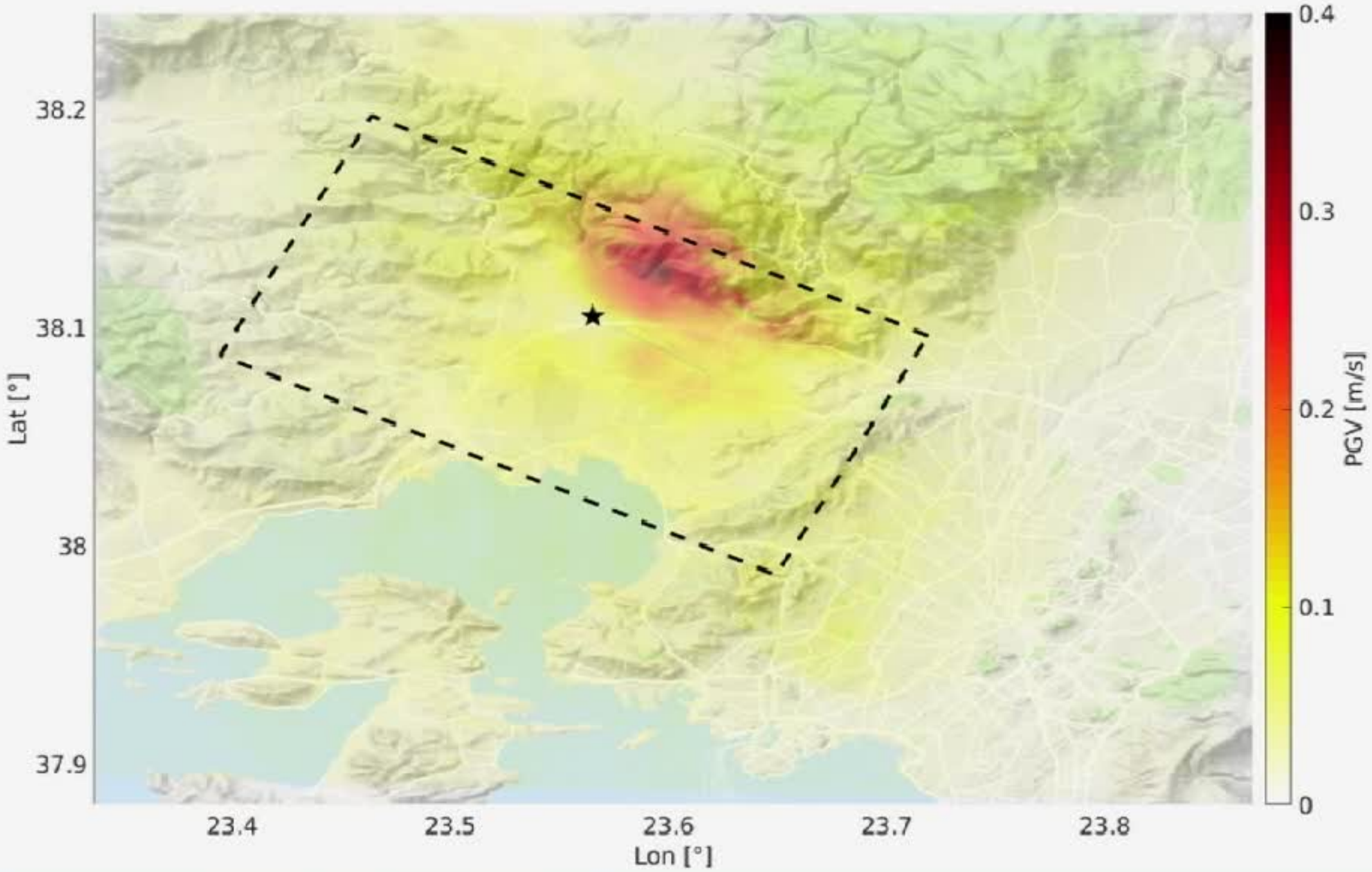

M 5.9 Athens Earthquake 1999

2000x exaggeration

Fili Fault

Athens

Fili Fault

Acropolis

PGV m/s

Max

Min

Elapsed time: 18.0 seconds

http://speed.mox.polimi.it

Synthetic ground motion scenarios: Istanbul and the Marmara Sea region

Synthetic ground motion scenarios: Istanbul and the Marmara Sea region

Computational model

Numerical model of Istanbul (resolution: f_{max}= 1.5 Hz)

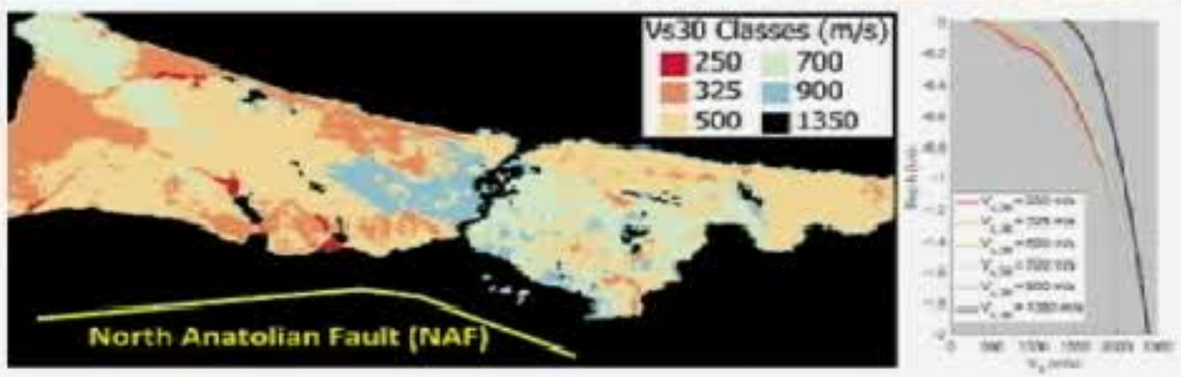

Horizontally stratified crustal model

Depth (km)	$C_s[m/s]$	Q
0-5	Fig. 3	V_S /10
5-10	3490	350
10-20	3500	350
20-30	3920	400

$$Q \approx \frac{1}{\zeta}$$

Computational model

Hexahedral elements	2.257.482
Degrees of freedom	~500 million
Frequency range	0 to 1.5 Hz
Element size range	180 m to 2 km

- Digital elevation model and map of classes of $V_{s,30}$ implemented in SPEED

Computed velocity fields for different scenarios

Velocity for different scenarios

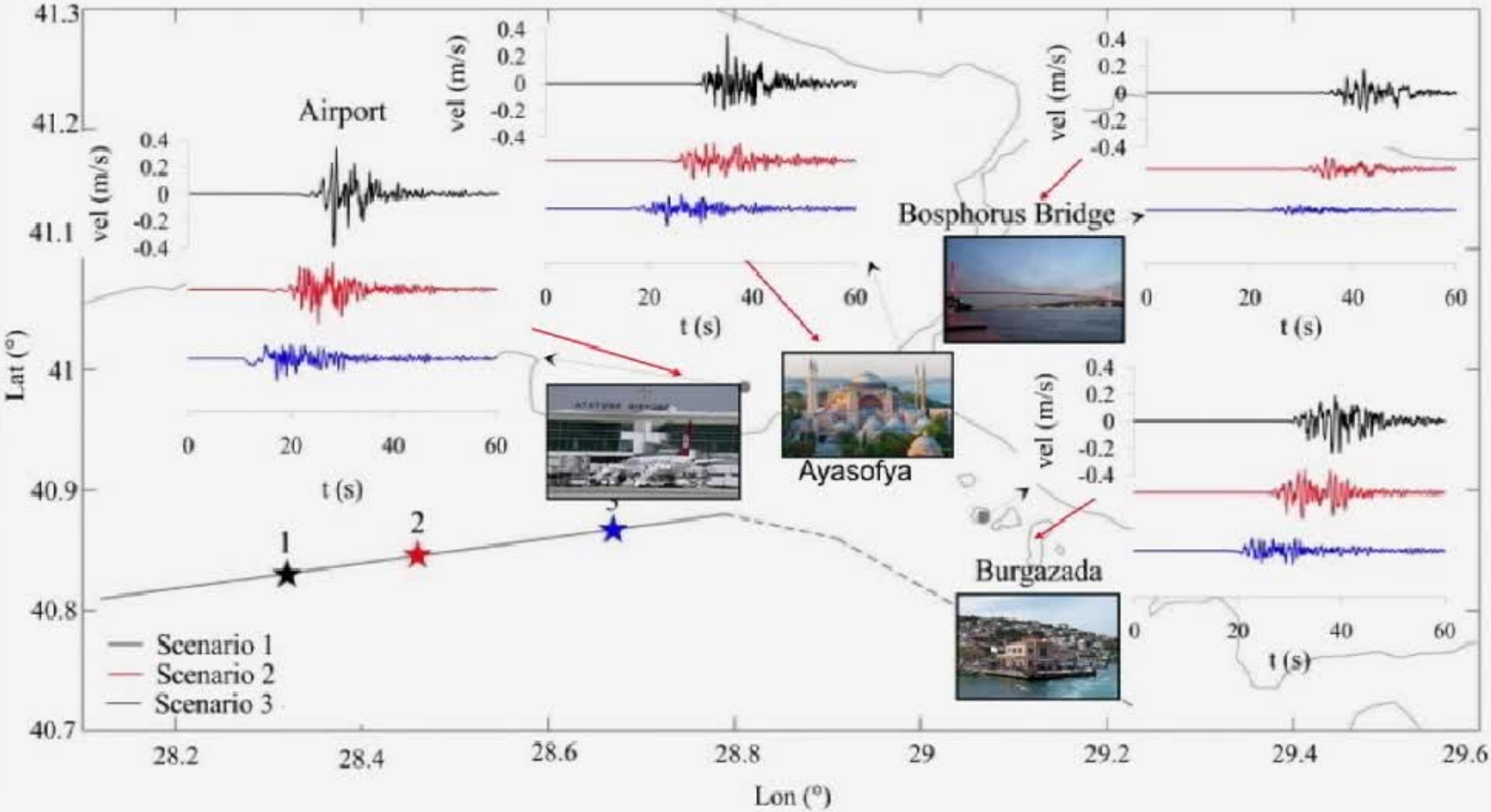

E00508

Time: 0,0 s

M 7.0

E00509

Time: 0,0 s

M 7.0

E00511

Time: 0,0 s

M 7.0

FO=fault orthogonal

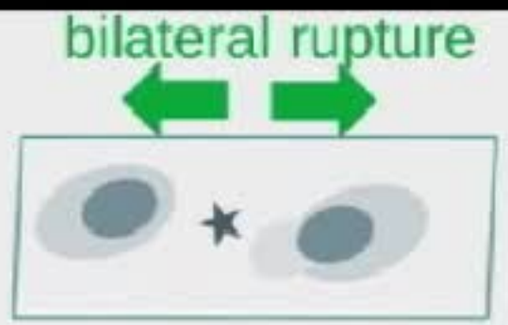

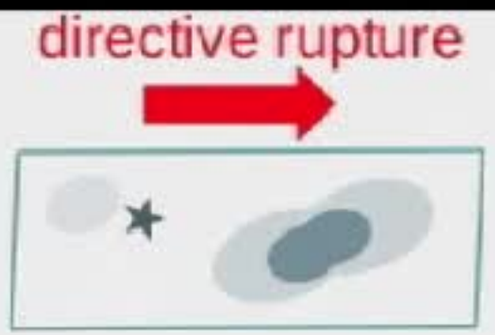

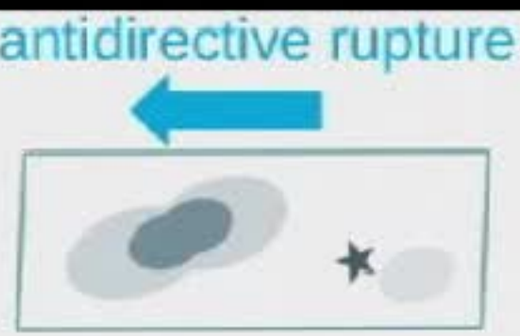

Computational model

Numerical model of Istanbul (resolution: f_{max}= 1.5 Hz)

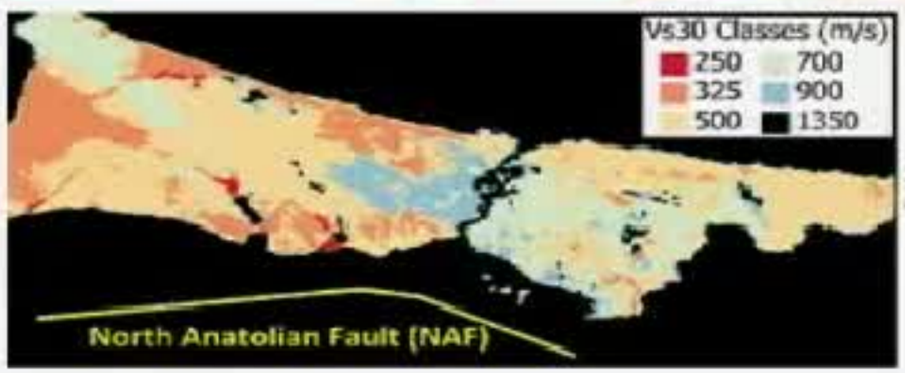

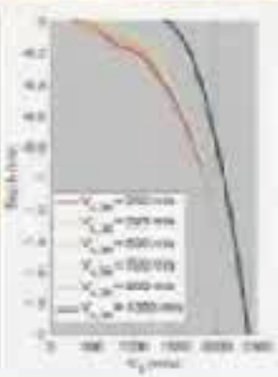

Horizontally stratified crustal model

Depth (km)	$C_s[m/s]$	Q
0-5	Fig. 3	V_S /10
5-10	3490	350
10-20	3500	350
20-30	3920	400

$$Q \approx \frac{1}{\zeta}$$

Computational model

Hexahedral elements	2.257.482
Degrees of freedom	~500 million
Frequency range	0 to 1.5 Hz
Element size range	180 m to 2 km

- Digital elevation model and map of classes of $V_{s,30}$ implemented in SPEED

E00508

Time: 32,2 s

M 7.0

E00509

Time: 32,2 s

M 7.0

E00511

Time: 32,2 s

M 7.0

FO=fault orthogonal

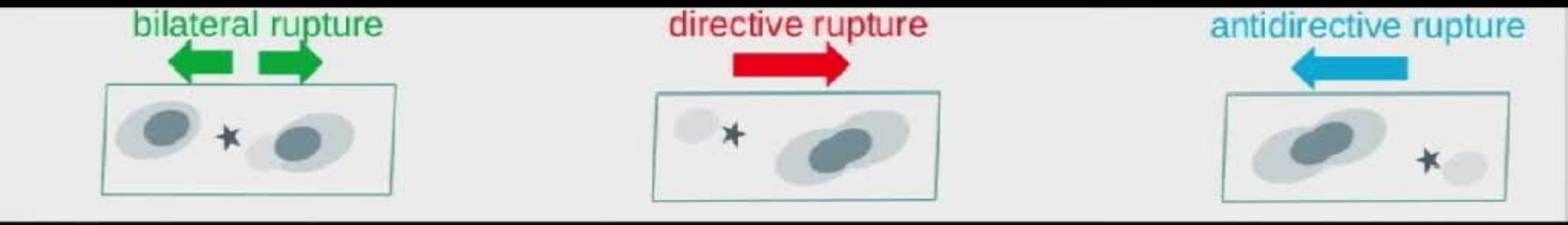

Computed velocity field for different scenarios

Velocity for different scenarios

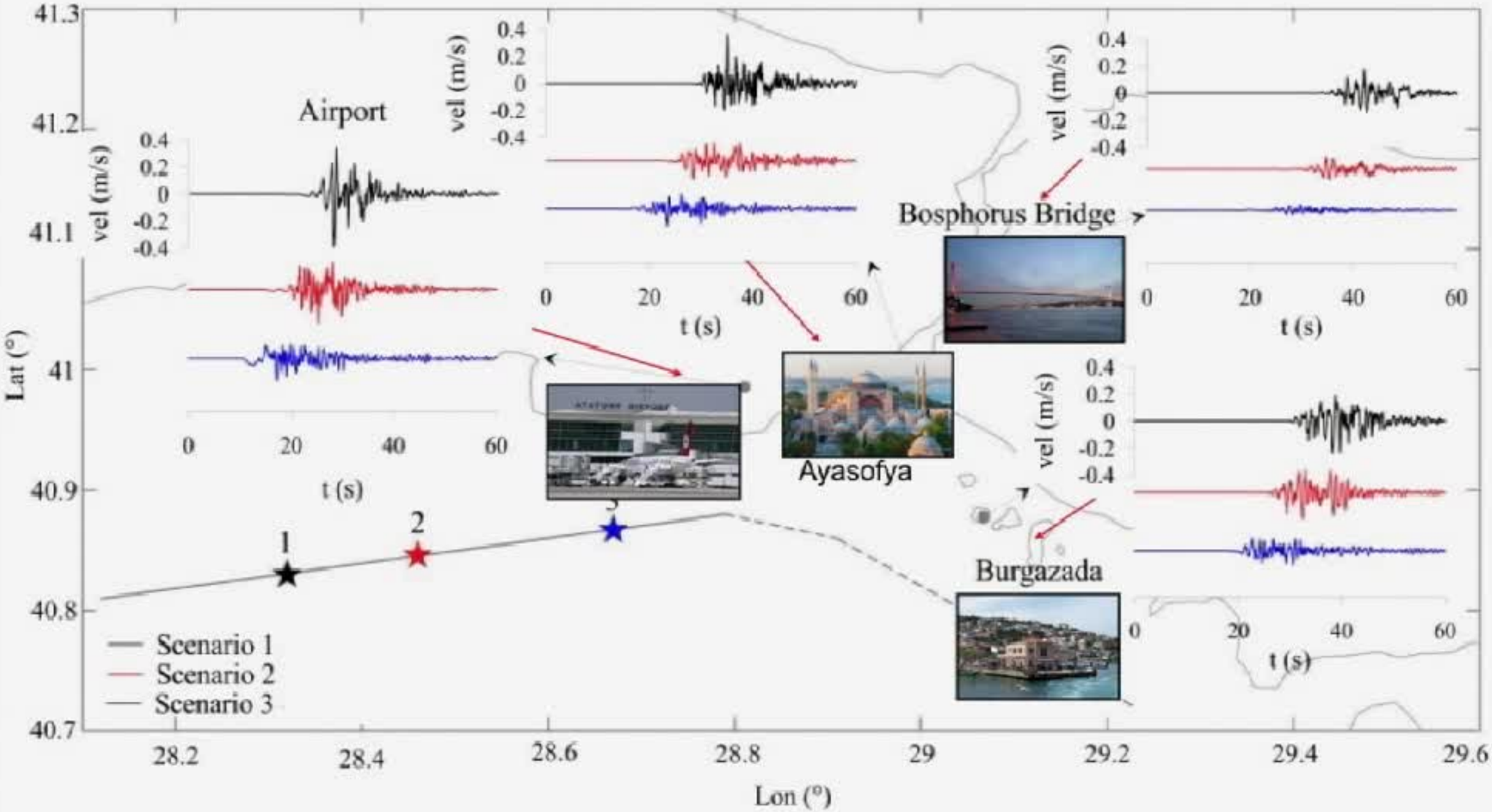

Synthetic ground motion scenarios: the Beijing metropolitan area

3D physics-based numerical modelling of Beijing

Beijing metropolitan area
Land: 16.801 km²
Popolation: 21.707.000
Density: 1.300/km²

Main features of the computational model

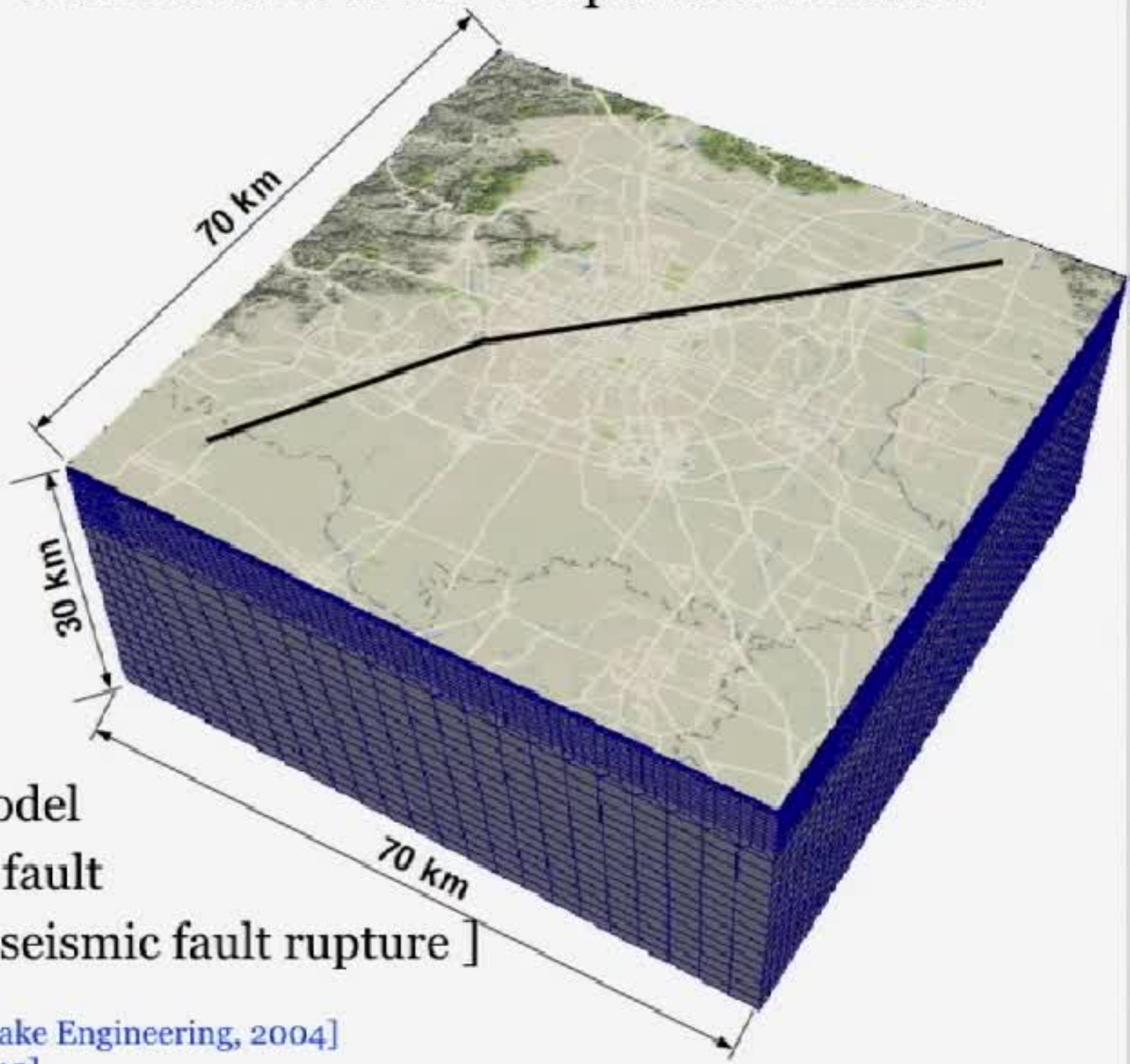

- Topography and 3D basin model
- Shunyi-Qianmen-Liangxiang fault
- Kinematic description of the seismic fault rupture]

[Gao, Yu, Zhang, Wu, Conference on Earthquake Engineering, 2004]
[Crempien, Archuleta, Seismol. Res. Lett., 2015]

Ground motion parameters: spectral displacement

1D building model subject to an earthquake

m :mass of the building
k :elasticity constant
c :dumping parameter
$u_3(t)$: ground motion displacement at the base of the building
$x_3(t)$: displacement of the building

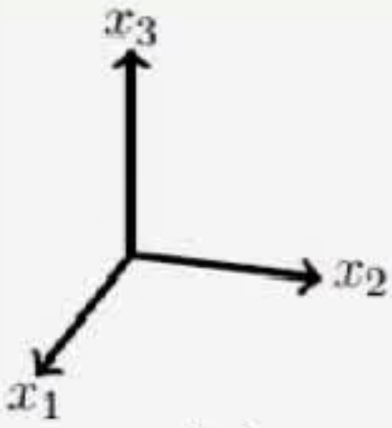

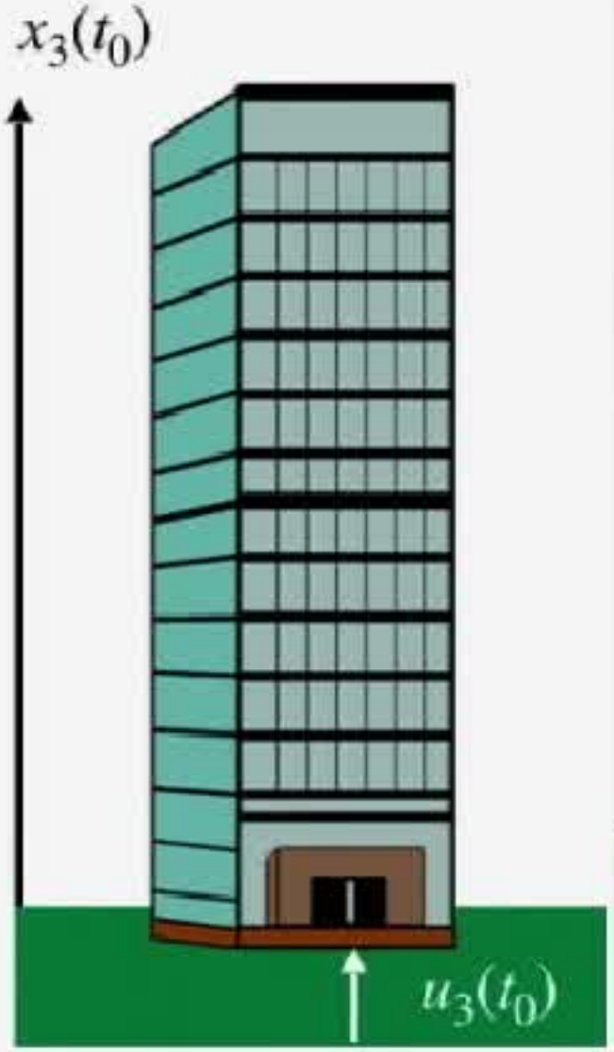

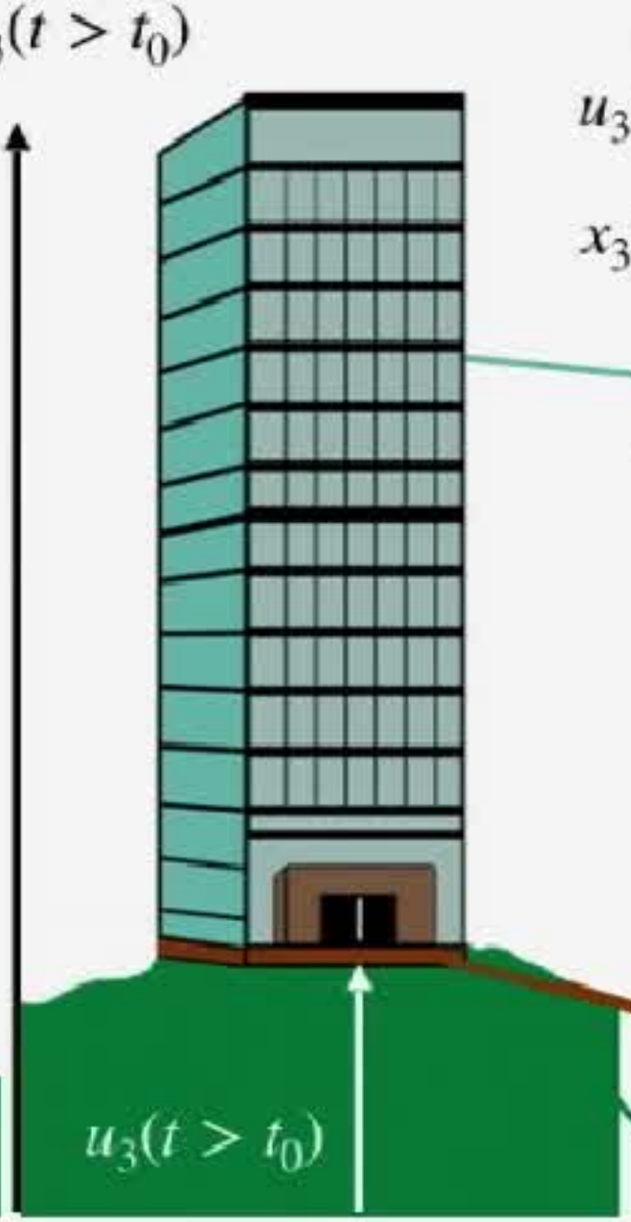

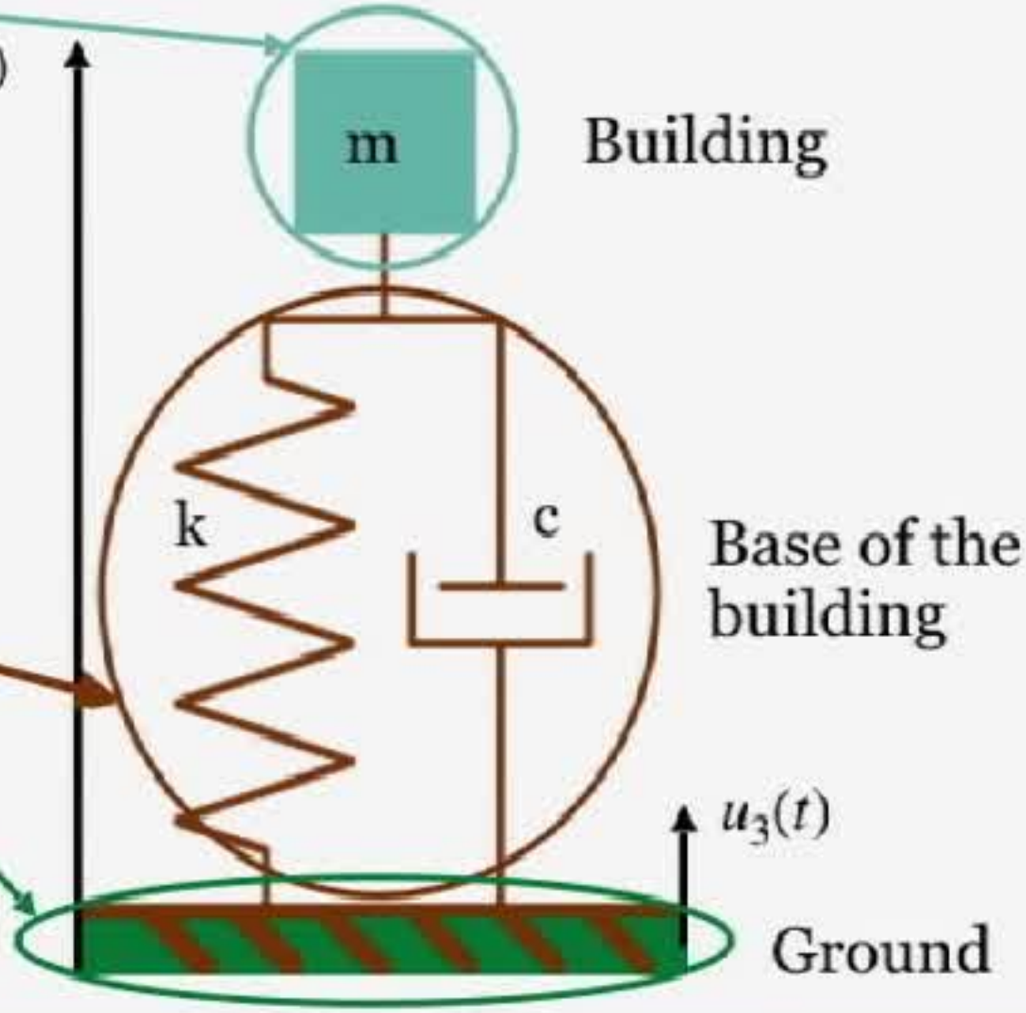

From SPEED to ground motion parameters

SD is the maximum relative displacement response of the building w.r.t. the ground

Spectral displacement (horizontal geometric mean) is a measure of the intensity of the earthquake and it is defined as

$$SD(\boldsymbol{x};T,\xi) = \sqrt{SD(x_1;T,\xi)SD(x_2;T,\xi)},$$

where $SD(x_1;T,\xi)$, $SD(x_2;T,\xi)$ are the spectral displacement computed w.r.t. x_1 and x_2 direction, respectively.

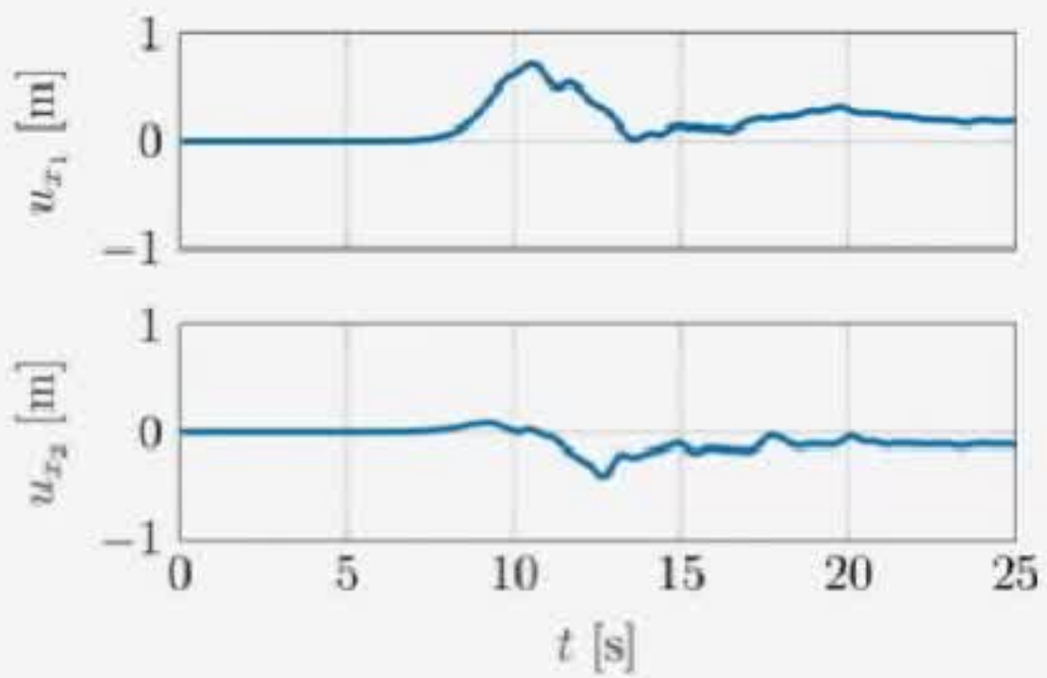

Input for dumped vibrating system:

- $\boldsymbol{u}(t), \ddot{\boldsymbol{u}}(t)$ computed displacement and acceleration in x_1, x_2 directions (by SPEED)
- T, ξ period and damping ratio (user-defined)

Output from dumped vibrating system:

$\boldsymbol{x}(t)$ displacement in x_1, x_2 directions of a dumped vibrating system, e.g. buildings.

Objective: compute $SD(\boldsymbol{x};T,\xi)$

From SPEED to ground motion parameters

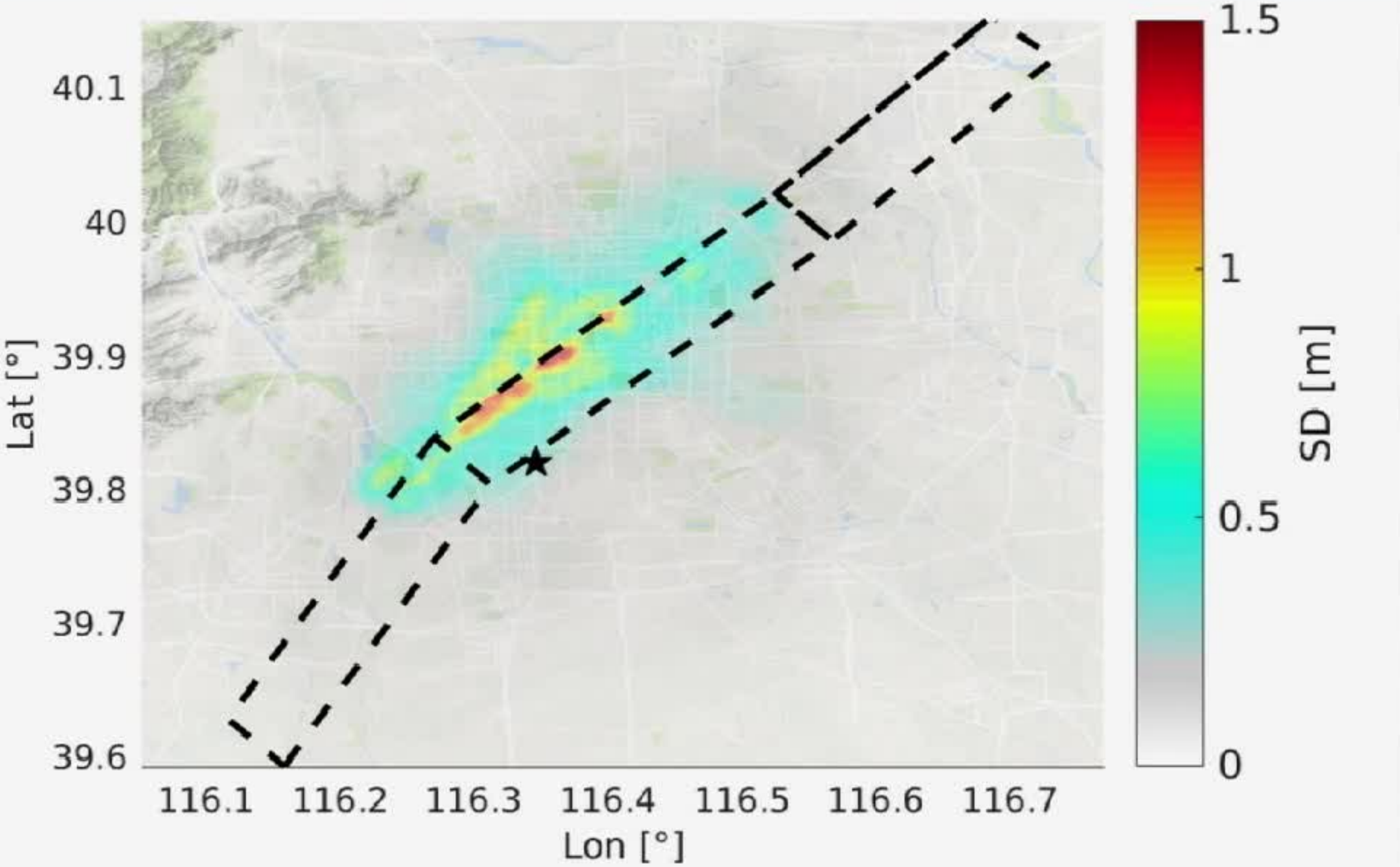

Spectral displacement (SD) map for $T = 3s, \xi = 0.05$

Seismic fragility curves model

Seismic fragility curves: represent the conditional probability of failure of constructions, e.g. buildings or bridges, for a given seismic response parameter, e.g. spectral displacement, peak ground acceleration, ...

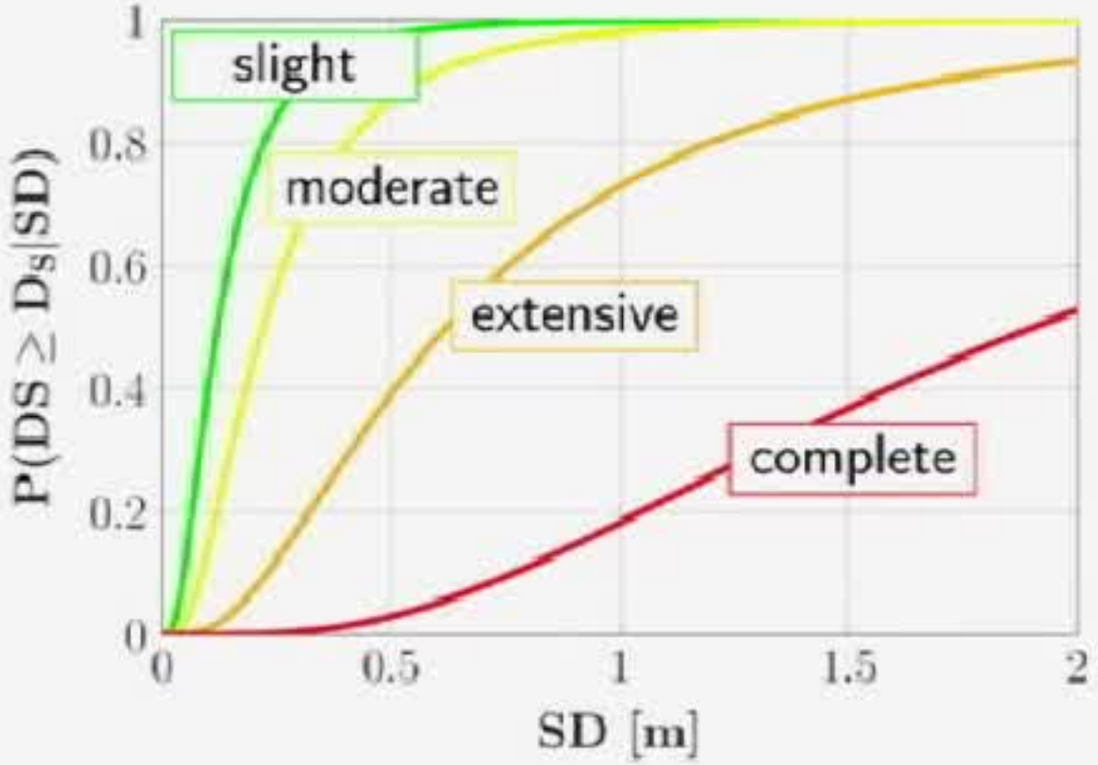

Profiles of fragility curves, i.e.,

$$P(DS \geq D_S|SD)$$

versus SD, for Chinese high-rise buildings. Each color denotes the type of damage state D_S.

Fragility curves for constructions are calibrated on their characteristics. E.g. for buildings: period of construction, material, storey numbers, ...

- DS = damage state variable: measures the damages of a construction in a qualitative way.
- D_S = type of damage state (slight, moderate, extensive, complete)
- SD = spectral displacement

[Wu, Wang, Yang, Appl. Mech. Mater., 2013]

Seismic risk analysis for high-rise buildings (100 - 200 m tall)

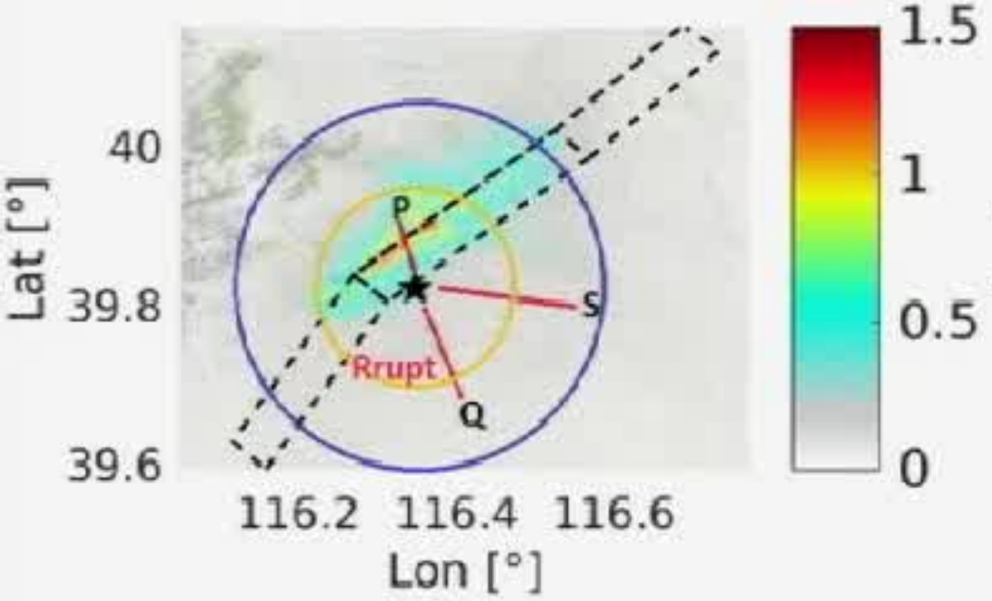

1. From the points *P, S, Q* with coordinates *(Lon, Lat)* compute the distances to the fault rupture area (Rrupt);
2. SD(Lon, Lat) ⟶ SD(Rrupt);
3. Subdivision of points *P, S, Q* in groups w.r.t. *Rrupt*.

Fragility curves

- **Colors** denote the probability of reaching a selected damage state, i.e., $P(DS = D_S)$, versus *Rrupt*.
- **Black dots** represent the mean of the probability of exceeding different damage states, i.e., $P(DS \geq D_S)$ versus *Rrupt*,
- **Black bars** represent the corresponding standard deviation.

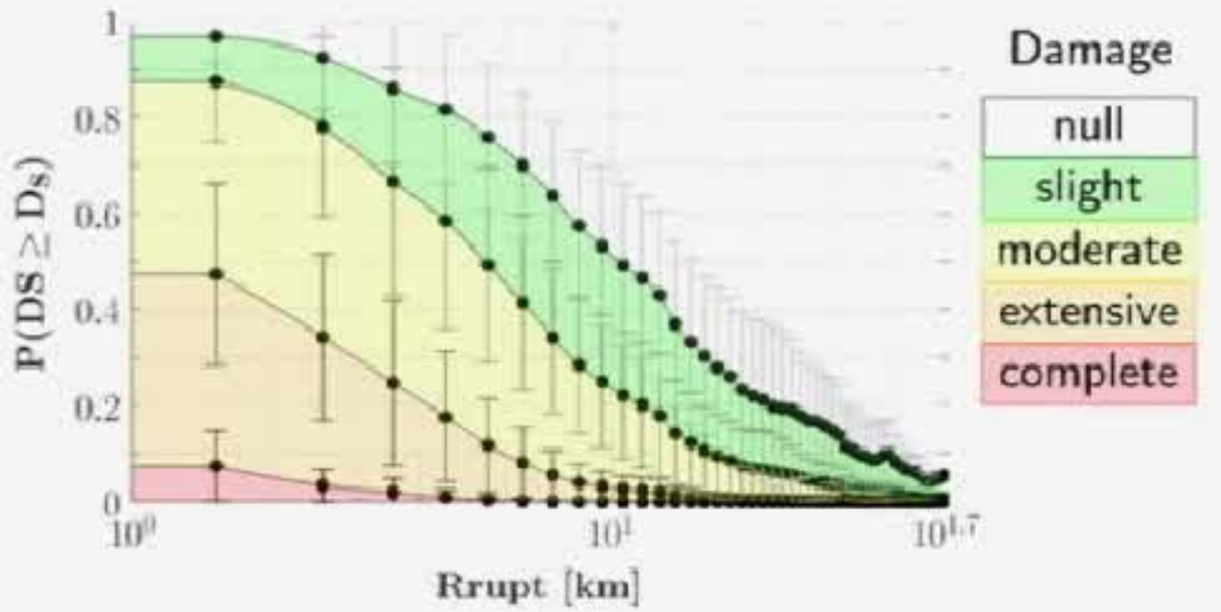

[Mazzieri, Melas, Smerzini, Stupazzini. Proceedings of the 16th European Conference on Earthquake Engineering. 2018]
[Antonietti, Mazzieri, Melas, Paolucci, Quarteroni, Smerzini, Stupazzini, in prep, 2019]

Christchurch earthquake
Mw 6.3

22 February 2011 at 12:51 p.m.

Dipartimento di **Ingegneria Civile e Ambientale**

Alfio Quarteroni

EPFL Lausanne & Politecnico di Milano

Christchurch earthquake

Mw 6.3

22 February 2011 at 12:51 p.m.

Alfio Quarteroni

EPFL Lausanne & Politecnico di Milano

Christchurch earthquake

Mw 6.3

22 February 2011 at 12:51 p.m.

Alfio Quarteroni

EPFL Lausanne & Politecnico di Milano

Christchurch earthquake
Mw 6.3

22 February 2011 at 12:51 p.m.

Alfio Quarteroni

EPFL Lausanne & Politecnico di Milano

Christchurch earthquake

Mw 6.3

22 February 2011 at 12:51 p.m.

Alfio Quarteroni

EPFL Lausanne & Politecnico di Milano

Christchurch earthquake
Mw 6.3

22 February 2011 at 12:51 p.m.

Alfio Quarteroni

EPFL Lausanne & Politecnico di Milano

Christchurch earthquake

Mw 6.3

22 February 2011 at 12:51 p.m.

Christchurch earthquake

Mw 6.3

22 February 2011 at 12:51 p.m.

Alfio Quarteroni

EPFL Lausanne & Politecnico di Milano

Christchurch Earthquake February 22, 2011

Christchurch Earthquake February 22, 2011

Christchurch earthquake

Mw 6.3

22 February 2011 at 12:51 p.m.

Alfio Quarteroni

EPFL Lausanne & Politecnico di Milano